Received: 3 January 2023 | Revised: 28 June 2023 | Accepted: 17 October 2023

DOI: 10.1002/cne.25559

RESEARCH ARTICLE

JCN RESEARCH IN SYSTEMS NEUROSCIENCE THE JOURNAL OF COMPARATIVE NEUROLOGY WILEY

# The neurovascular unit of capillary blood vessels in the rat nervous system. A rapid-Golgi electron microscopy study

Jorge Larriva-Sahd | Gema Martínez-Cabrera | Carlos Lozano-Flores | Luis Concha | Alfredo Varela-Echavarría

Campus Juriquilla, Instituto de Neurobiología Universidad Nacional Autónoma de México, Querétaro, México

**Correspondence**
Jorge Larriva Sahd, UNAM, Campus Juriquilla, Blvd. Juriquilla 3001, Juriqulla, Qro, CP 76230, Mexico.
Email: jlsneuro@unam.mx

**Funding information**
Laboratorio Nacional de Visualización Científica Avanzada; Alejandro de León Cuevas; Alejandro Ávalos Fernández; Luis A. Aguilar Bautista; Adriana González Gallardo; Michael Jeziorsky Ma. Antonieta Carbajo; Loudes Palma; Martín García Servín; Instituto de Neurobiología, UNAM

## Abstract

We describe a pericapillary organ in the rat forebrain and cerebellar cortex. It consists of a series of tripartite synapses with synaptic extensions enveloped by astrocytic endfeet that are linked to the capillary wall by synaptic extensions. Reciprocal specializations of the pericyte-capillary blood vessel (CBV) with such specialized synapses suggest a mechanoreceptor role. In Golgi-impregnated and 3D reconstructions of the cerebral cortex and thalamus, a series of TSs appear to be sequentially ordered in a common dendrite, paralleled by synaptic outgrowths termed golf club synaptic extensions (GCE) opposed to a longitudinal crest (LC) from the capillary basal lamina (BL). Our results show that, in the cerebellar cortex, afferent fibers and interneurons display microanatomical structures that strongly suggest an interaction with the capillary wall. Afferent mossy fiber (MF) rosettes and ascending granule cell axons and their dendrites define the pericapillary passage interactions that are entangled by endfeet. The presence of mRNA of the mechanosensitive channel *Piezo1* in the MF rosettes, together with the surrounding end-feet and the capillary wall form mechanosensory units. The ubiquity of such units to modulate synaptic transmission is also supported by *Piezo1* mRNA expressing pyramidal isocortical and thalamic neurons. This scenario suggests that ascending impulses to the cerebellar and cortical targets are presynaptically modulated by the reciprocal interaction with the mechanosensory pericapillary organ that ultimately modulates the vasomotor response.

**KEYWORDS**
BOLD, mechanosensory, perivascular synapse, Piezo1

## 1 | INTRODUCTION

Processes involved in the control of brain circulation are too important to be overlooked (Roy & Sherrington, 1890). Because the viability of highly differentiated nerve cells relies upon the exchange of bioactive molecules with CBVs this process is of fundamental relevance. Although peripheral blood circulation appears to be chiefly controlled by the autonomous nervous and endocrine systems, cerebral blood supply is driven by different regulatory mechanisms (Roy & Sherrington, 1890). More specifically, researchers have assumed that the motor control of capillary blood flow relies on the neurotransmitter, cranial nerve, and central aminergic systems innervating tributary muscular arteries because no meningeal nerve fibers penetrate beyond Robbin–Virchowt's space (Jones, 1970). Hence, capillary blood flow results from the passive reception of arterial blood, whereas motor activity is virtually absent. A fundamental concept for the present study is the widespread observation that neuronal or receptor (Chaigneau et al.,

**Abbreviations:** AP, asymmetric process; BL, basal lamina; CBV, capillary blood vessel; GCE, golf club synaptic extension; iBL, inner basal lamina; LC, longitudinal crest; MF, mossy fiber; NCU, neuro-glial capillary unit; oBL, outer basal lamina.

  

2003) recruitment within discreet areas of the cerebral cortex leads to a rapid increase in blood flow that ceases as the stimulus ends (Cauli & Hamel, 2010). This neurovascular coupling is the cornerstone of functional magnetic resonance imaging (Bandettini et al., 1992; Grinvald et al., 1991; Ogawa et al., 1992). Although the mechanisms that initiate the hemodynamic response have been documented (Iadecola, 2017; McCaslin et al., 2011), an important question remains involving how the intended effect (i.e., an increase in blood flow) feeds back to the motor pool. Incidentally, most motor and endocrine systems, which are initially thought to be exclusively efferent, possess feedback mechanisms via sensory organs or hormones. In consideration of this scenario, it has been assumed that the orchestrated interaction of endothelial cells, astrocytes, and neurons enables subtle capillary blood flow variation, to tune the motor limb of the circuit (Armulik et al., 2010; Idecola, 2004, 2017; Iadecola & Nedergaard, 2017; Moore & Cao, 2008; Reichenbach & Wolburg, 2005; Tsvetanov et al., 2020; Zonta et al., 2002). Nonetheless, researchers failed to define the substrate(s) linking them. More precisely, there is a question as to which sector(s) of the vascular tree between arterioles and terminal arterial capillaries are responsible for capillary blood flow regulation. This question is a matter of debate (Armulik et al., 2010; Iadecola & Nedergaard, 2017). Over the past decade, we have investigated the perivascular neuropil and initially described a set of neurons within the brain vasculature (specifically within arteries). The long processes of these unique perivascular neurons are associated with granule-containing, tuberous structures at sites of ramifying blood vessels that appear to correspond to mechanoreceptors (Larriva-Sahd et al., 2019). Because the perivascular neurons and their processes are absent in capillaries with diameters of 15 μm or less, we decided to study the structure of the brain–CBV interphase. Although the EM-3D descriptions of CBVs and associated neural and glial processes are available (Mathiisen et al., 2010; Rechenbach & Herting, 2010; Shapson-Coe et al., 2021), a systematic search for structural specializations between them is necessary. Hence, the first goal of the present study was to revisit the structure of the capillary wall and neighboring neuropil of the forebrain and cerebellar cortex with light and electron microscopy. This allowed for the identification of a novel series of synaptic, dendritic, and astroglial specializations associated with the capillary wall. Furthermore, neuronal sources of pericapillary processes and mRNA expression to *Piezo1* were defined.

## 2 | MATERIALS AND METHODS

### 2.1 | Golgi technique

Brains from normal, pathogen-free adult Wistar rats ($n = 25$) were raised in our vivarium facility with free access to food and water. Animal handling, anesthesia, and sacrifices were performed according to our "Comité de Ética del Instituto de Neurobiología," Code 2016–60. Perivascular cells, interstitial ground substance, and nerve fibers structuring the neurovascular unit (Hawkins & Davis, 2008) were assessed. Briefly, after sacrifice with a barbiturate overdose, brains were removed from the skull and transversely cut into equidistant quarters with a sharp pair of scissors. Tissue blocks (approximately 4-mm thick) were sampled from the brain stem, cerebellum, frontal and parietal isocortices, hippocampus-entorhinal cortex, diencephalon, basal ganglia, olfactory cortex, olfactory bulb, and olfactory peduncle. Each sample was placed in an aqueous solution containing 0.25% osmium tetroxide and 3% potassium dichromate for 10–13 days and transferred to a 0.75% silver nitrate solution for incubation for 20 additional days. Additionally, each block of tissue was encased with a paraffin shell and serially sectioned at a thickness of 150 μm with a sliding microtome. Sections were transferred to 70% ethyl-alcohol, dehydrated, cleared with terpineol-xylene, mounted, numbered, and coverslipped with Entellan (Merck). Species conservation of the pericyte and its processes was assessed in specimens of adult mouse, rat, hamster, rabbit, and rhesus monkey from our archives. Images were obtained by using a camera lucida adapted to an Axioplan 2 (Zeiss) light microscope, via 40X and 100X oil objectives. Indian ink and soft pencil drawings were obtained from representative areas. Furthermore, somatic, axonal, dendritic, and vesicular structures were measured in digital images acquired with an AxioCam camera by using Kontron software (Zeiss). Illustrative light microscopic images from Golgi-impregnated specimens were obtained by overlapping a variable number of sharp focus areas into a single micrograph.

### 2.2 | Electron microscopy

Brains from five adult rats, similar to those in section 2.1, were used for this part of the study. Subjects were deeply anesthetized and perfused through the left ventricle with Karnovsky's fixative and processed as previously described (Larriva-Sahd, 2006, 2008; Varela-Echevarría et al., 2017). Tissue blocks of approximately 1-mm thick from the frontal and parietal isocortices, posterior thalamus, and cerebellar cortex were dissected out, according to Swanson's atlas (Swanson, 2004). Samples of tissue were postfixed for 1 h in 1% osmium tetroxide dissolved in 0.1 M cacodylate-HCl buffer; subsequently, they were dehydrated in graded acetone and embedded in epoxy resin. Afterward, a 1-μm-thin section was obtained from the tissue blocks in a Leica ultramicrotome equipped with glass knives. Silver to gold-colored sections were obtained with a Leica ultramicrotome equipped with glass knives and mounted on copper grids. Last, sections were sequentially stained with uranium and lead salts and were observed under a JOEL 1010 electron microscope.

### 2.3 | Serial sectioning and 3D reconstructions

For tridimensional reconstructions tissue blocks from the adult rat, hippocampus, cerebral cortex, cerebellar cortex, primary olfactory cortex, thalamus, and olfactory bulb were used (Table 1). Series were obtained with Leica microtome equipped with a diamond knife. Successive 70- to 80-nm thin sections were mounted on one-slot copper grids that had previously been covered with Formvar film. Subsequently, specimens were sequentially stained with aqueous uranium and lead salts

**TABLE 1** Series observed via the electron microscopy and 3D reconstructions.

| Source | Number of series | Mean number of sections | Reconstructions |
|---|---|---|---|
| Cerebral cortex | 12 | 75 | 8 |
| Thalamus | 10 | 58 | 12 |
| Cerebellar cortex | 11 | 77 | 15 |

and observed under a JOEL 2020 transmission electron microscope. Areas of interest were serially photographed under the electron microscope with a Gatan digital camera. Then, images from each series were aligned first with ImageJ-FIJI software, free-hand outlined with a cursor, and then reconstructed with a software that is freely available (Reconstruct, http://synapses.clm.utexas.edu/tools/reconstruct/reconstruct.stm.). We used microtome diamond-cut series as they provide the superior resolution of the transmission EM as well as the opportunity to perform post hoc observation in series that otherwise is lost in gallium-sectioned specimens.

## 2.4 | Immunohistochemistry and in situ hybridization

### 2.4.1 | In situ hybridization

A fragment of the rat *Piezo1* cDNA was amplified with Taq Polymerase and the oligonucleotide primers 5′-GAGGAAGAGGACTACCTT and 5′-TTTACTTAGAAAACCCTACAG from bladder total RNA and cloned into the Pgem-T Easy vector (Promega). The sequence was confirmed using Sanger capillary sequencing, and sense and antisense RNA probes were synthesized with T7 and SP6 RNA polymerases (Roche-Sigma-Aldrich), respectively, as well as FITC-UTP (with FITC RNA labeling kit from Roche). These probes were then used for in situ hybridization on cryosections of fresh brain tissue that was snap-frozen in blocks of Tissue-Tek (Sakura) employing an isopentane bath cooled with powdered dry ice. Cryosections of 30 µm were obtained on SuperFrost Plus slides (Fisher-Scientific), and fluorescent in situ hybridization was performed as described (Hernández-Linares et al., 2019). FITC-UDP detection was performed by using a peroxidase-conjugated anti-FITC antibody (Roche) and FITC-tyramide signal amplification system (Akoya Bioscience). Fluorescent immunostaining was performed on cryosections obtained on Superfrost Plus slides of tissues fixed in 3.5% paraformaldehyde in PBS employing the antibodies of Tables 1 and 2. Immunostaining of vGlut (RRID: AB1603114) and calcitonin gene related protein (CGRP) was performed in cryosections of the cerebellum of mice expressing the reporter green fluorescent protein (GFP) under the control of the glial fibrillar acidic protein (GFAP) promoter (Jung et al., 2009; Nolte et al., 2001) as well as 4′,6-diamidino-2-phenylindole (DAPI) staining for nuclei and B4 isolectin (IB4) for CBVs (Table 3).

The fluorescence was depicted using a Carl Zeiss—LSM 880 Confocal microscope and ZEN software and Plan-Apo 63x N.A. = 1.4 oil immersion objective. The 3D images were obtained in Z-stacks from 30 to 40 µm of depth with 1024 × 1024 pixels of resolution and analyzed with the image-processing package Fiji (version: 2.0.0-rc-66/1.52b; http://imagej.net/contributors) of the ImageJ program and Amira Software (https://www.thermofisher.com/mx/es/home/electron-microscopy/products/software-em-3d-vis/amira-software.html).

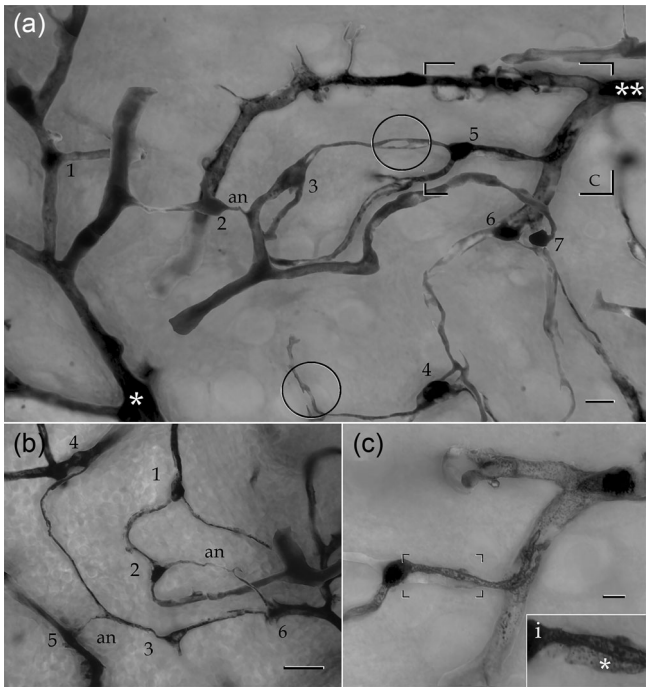


**FIGURE 1** Photomontages of blood vessels and associated pericytes (PCs) in the mouse cerebral cortex. (a) Survey micrograph of a capillary bed arising from a penetrating arteriole (*) converging into a penetrating venule (**). Seven PCs extend their processes in close apposition to the capillary wall. Note that the processes of most PCs (3–5) form lineal series (see text), whereas others (2) form a tangential shunt as they course devoid of a CBV. Two mesh processes (circles) are clearly observed. Hippocampal cortex. (b) PCs with processes that organize into lineal (1 and 2) and diagonal (2 and 3) interactions. Note that the latter relay upon perforating processes (an) devoid of an associated CBV. Hippocampal cortex. string process. (c) Bipolar PC, cell 5 in "A" sending paired primary processes coursing along the capillary wall. (i) High-magnification view of that portion of the SP outlined in "C." Note the flat, membranous appendage (*) forming a secondary process. Calibration bars = 30 µm in (a), 10 in (b) and (c); 5 in "i."

## 2.5 | Nomenclature and information retrieval

We adopted rigid, accepted criteria to define CBVs. Under the light microscopy, CBVs plexuses are considered as those vessels arising from terminal arterioles of less than 15 µm (McDonald & Larue, 1983) and leading to postcapillary veins. The higher affinity for silver and smaller caliber of the former vessels allows for the unambiguous differentiation from the latter vessels (Figure 1a). Under the electron microscope, the CBV is considered a vessel with a diameter of < 5 µm, surrounded

**TABLE 2** List and characteristics of primary antibodies used in immunohistochemistry.

| Primary antibodies | | | | | |
|---|---|---|---|---|---|
| **Name** | **Host** | **Clonality** | **Dilution** | **Catalog #/ID** | **Manufacturer** |
| vGlut2 | Mouse | Monoclonal | 1:500 | Ab79157/AB1603114 RRID: AB1603114 | Abcam |
| Anti-fluorescent-POD | Sheep | Monoclonal | 1:1000 | 11426346910, RRID:AB_840257 | Roche |

**TABLE 3** Secondary antibodies used to visualize sites immunoreactive to primary antibodies.

| Secondary antibodies | | | | | | |
|---|---|---|---|---|---|---|
| **Name** | **Host** | **Conjugate** | **EX/EM (nm)** | **Dilution** | **Catalog #/ ID** | **Manufacturer** |
| Anti-mouse | Donkey | Alexa-Fluor 594 | 590/617 | 1:1000 | Ab-2813898 RRID:AB2813898 | Abcam |

by pericytes with cytoplasm devoid of myofibrils and/or electron-dense submembrane clusters of myofibrils, which are typically observed in myocytes (Hill et al., 2015). With these guidelines, consistent CBV identification was performed.

## 3 | RESULTS

As previously described (see Larriva-Sahd et al., 2019), intrinsic arteries of the brain, possessing medium to large calibers, are encased by a distinct set of cells or perivascular neurons that are likely to furnish a sensory network. Currently, no perivascular neurons have been found in the capillary bed. However, distal to the pericapillary arterioles, smooth muscle fibers were replaced by pericytes so that they formed a continuous cellular network surrounding CBVs (Figure 1). Although thorough descriptions of the structure of the pericyte are available, a brief description is desirable to provide the context for undescribed characteristics. The nomenclature suggested earlier (Sims, 1986; Zimmermann, 1923) for the pericyte and its processes will be used throughout the text. The soma and processes of the pericyte that were visualized in Golgi-stained specimens of the adult rat are summarized in Figures 2 and 3.

Pericytes (PCs) form a single row encasing virtually all the CBVs throughout the brain (Sims, 1986; Ushiwata & Ushiki, 1990). Aside from occasional, narrow gaps between them (Berthiaume et al., 2018), distal processes from adjacent pericytes typically overlap with each other or with endfeet (see Section 3.3; Figure 4b). When CBV plexuses are tracked from precapillary arterioles to postcapillary venules, the extent of the pericyte covering becomes evident (Figure 1a,b). Alternatively, isolated vessels or small groups of vessels with diameters of less than 6 μm can reliably be considered CBVs (Figures 1, 3, and 4).

### 3.1 | The pericyte

Characteristics of the pericyte and its processes are shown in Figures 1–3 and 4b. The protruding perikaryon of the pericyte is located either at sites of CBV ramification or in the ensuing capillary shaft and in order of frequency; moreover, two or three primary processes arise from the pericyte cell body (Figures 1 and 2a). These processes are dark and elliptical, coursing parallel to underlying CBV for lengths that vary from 20 to 200 μm. Two types of processes are usually identified in the pericyte: specifically, a dark, argentaffin extension (or primary process) and a process with light, flat digitations (or a secondary process). The former type is oval or cylindrical, whereas the latter type is flat, and its finger-like outgrowths exhibit marked pleiomorphism (Figure 3b,c), thus recapitulating those characteristics observed with scanning electron microscopy in muscular (Mazanet & Franzini-Armstrong, 1982), glandular (Fujiwara & Uehara, 1984), or cerebral (Ushiwata & Ushiki, 1990) CBVs. A third distinct development, or "asymmetrical process" (AP), results from the uneven ramification of a primary process (Figures 1a, 2a, and 3b) and will be further described in a later section. Under the electron microscope (Figure 5), the pericyte cell body was rounded or triangular; moreover, although its contour was generally smooth, numerous short, pleomorphic outgrowths occasionally overlapped with those arising from presumptive neighboring pericytes (Figure 5e–g). CBV gaps devoid of pericyte coverage are indistinct. The pericyte nucleus exhibited an overall oval or horseshoe shape, and its longest axis adapted to the capillary contour (Figure 5a,c). Like peripheral CBVs, the cerebral pericyte and its processes remain confined to that area bounded by the inner basal lamina (iBL) and outer basal lamina (oBL) leaflets of the capillary basement membrane (Figure 5a,c; Burns & Palade, 1968). Additionally, the so-called fluorescent

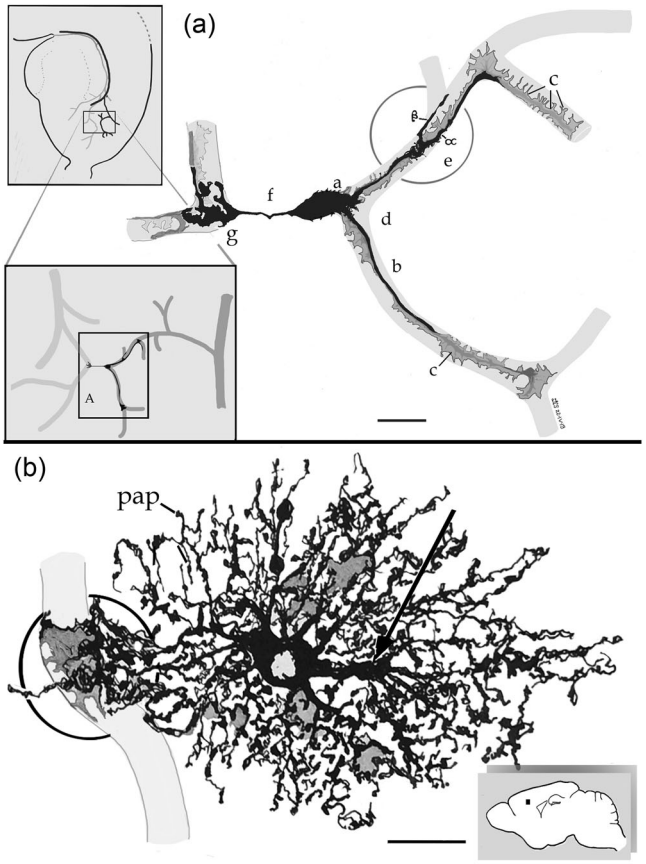


**FIGURE 2** Camera lucida drawings from pericapillary cells and their processes. (a) The perikaryon of a PC (a) gives rise to three divergent processes with two of them encircling the capillary contour (light gray), and a third one, orstring processes (f), coursing throughout the neuropil to reach an homolog by the terminal vesicular complex (g). b = primary process; c = secondary process; e = asymmetric process (AP). Note the two branches structuring the AP, including a short branch ($\beta$) and a long branch with membranous outgrowths ($\alpha$). (b) A protoplasmic astrocyte in the cerebral cortex originating, proximal or paraxial-processes (Varela-Echevarría et al., 2017), an endfoot (circle) and numerous peripheric astrocytic processes. Soft pencil = CBV (soft pencil). Scale bars = 3 μm.

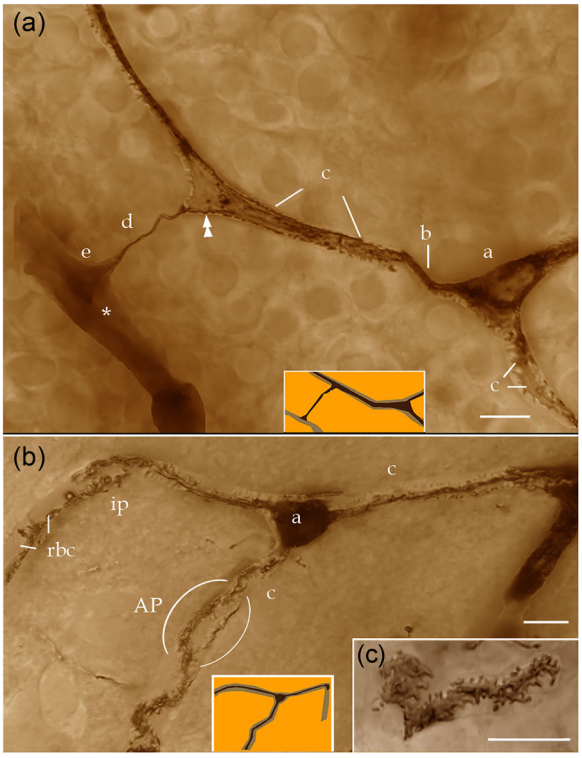


**FIGURE 3** High-magnification photomontages of the PC and its processes. (a) The triangular perikaryon of a PC (a) originates divergent processes encircling the unstained capillary wall (light brown-colored in the image). A primary process (b) gives rise to a secondary process (c), which correspondingly sends an orthogonal string process (d) piercing the neuropil to form a terminal vesicular complex (e) at the wall of the nearby CBV (*). Notice that the string process may be tracked back to the cytoplasm (double arrowhead) of the parent process. (b) Photomontages of the PC and its processes. Tripolar PC (a) riding on a branching CBV. The thick, divergent secondary processes (c) encircle the external aspect of the unstained CBV, which appears lighter and contains the ghost of red blood cells (rbc). Ramification of a secondary process originating an AP can be observed (ellipse). (c) High-magnification, in the face view of secondary processes. Note the short, transverse outgrowths (arrowheads). Scale bars = 5 μm.

granular perithelial cell (Mato et al., 1984) that is described in later sections shares with the pericyte an area bounded by the iBL and oBL. Characteristics of the cell nucleus and surrounding pericyte cytoplasm are presented in the panels in Figure 5. Briefly, organelle distribution within the perikaryal cytoplasm is asymmetrical (Figure 5a–c). Thus, one pole of the perikaryon is organelle-rich (Figure 5b–d) and contains numerous mitochondria, rough endoplasmic reticulum, and one or two small Golgi apparatus organelles, all of which are surrounded by scattered ribosomes and glycogen particles. The opposite pericyte pole is an organelle-poor area (Figure 5e) with a contour that frequently interdigitates with the plasma membrane of a penetrating pericyte process. Electron microscope series also demonstrates that the perikaryal profile exhibits numerous in- and out-growth reciprocating processes of a neighboring pericyte. Similar interweaving interactions are also observed in juxtaposed distal processes. These membrane-to-membrane interactions are commonly sealed by alternating tight junctions (Burns & Palade, 1968; Figure 5e–g).

The protoplasmic astrocyte and its processes (Figure 2b) directly interact with the pericyte. More specifically, astrocytes give rise to a variable number of thick paraxial processes (Varela-Echevarría et al., 2017) ending in numerous, thin peripheral processes, and in large cytoplasmic enlargements or endfeet (EF) that encase the capillary wall.

### 3.1.1 | Interaction between pericytes: Lineal and tangential linkage

Lineal interactions result from the longitudinal, successive arrangement of pericytes along capillary shafts via junction complexes (see Section 3.1.2), whereas tangential bridges from a pericyte process

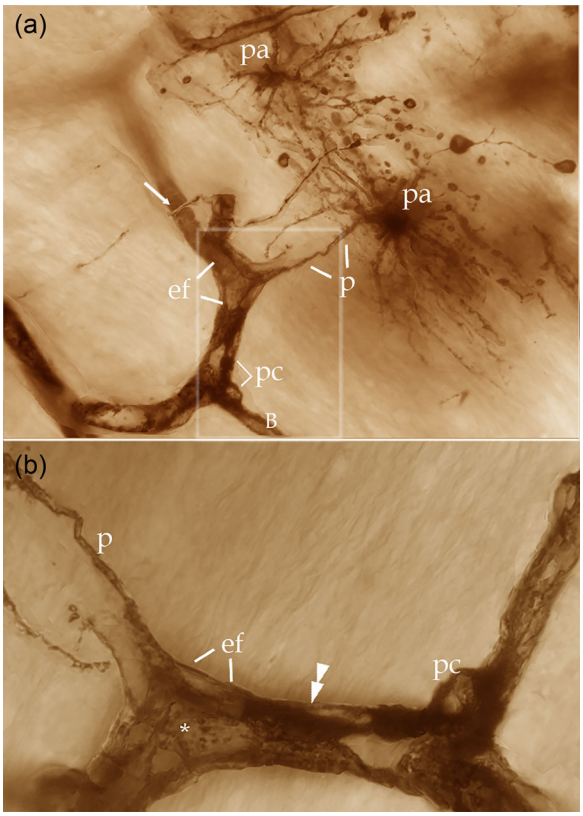


**FIGURE 4** Photomontages from the astrocyte and its processes. (a) Protoplasmic astrocytes with perikaryon (pa) that gives rise to numerous radial processes; one of the process (p) is longer and thicker and evolves to a triangular enlargement or endfoot (ef). The latter process embraces the capillary wall. (b) High-magnification view of the endfoot framed in "A." The mantle-like endfoot (ef) extends to cover both the ensuing mesh process (*) from a proximal process (double arrowhead) of the nearby PC (pc). Scale bars = 5 μm.

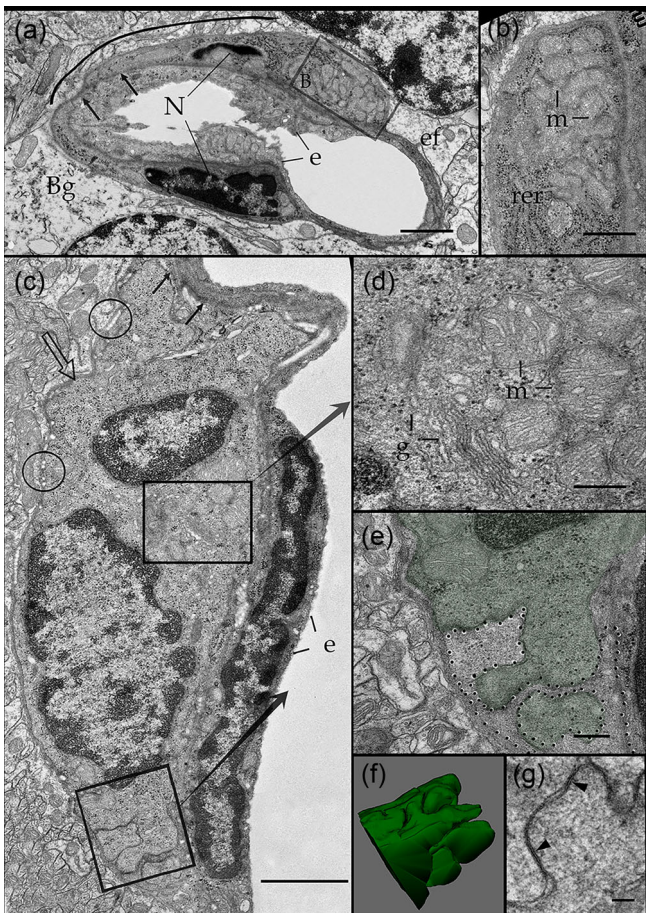


**FIGURE 5** Electron microscopic views of the PC: position and interaction with the capillary wall. (a) Cross-section of the root of two CBVs partially surrounded by the same PC with horseshoe-shaped nucleus that appears to be sectioned at either side of the endothelial cell cytoplasm (e). Note the BL, which splits into an inner (black arrows) and outer (hollow arrow) portion encasing the PC itself. The latter portion correspondingly, faces a Bergman glial cell (Bg) and astrocytic end-feet (ef), thus forming a long, interrupted covering exposing the outer BL, and opening to the neighboring neuropil (curved line). (b) Note the numerous mitochondria and (m) rough endoplasmic reticulum (rer) in a higher magnification view of that area of the perikaryon outlined in "A." (c) Longitudinal section through the capillary wall. Organelles contained by the central (center) and polar (lower) perikaryon of the PC. Notice the inner (black arrows) and outer (hollow arrow) BL containing rows of elastic fibrils (circles) also interacting with the neuropil as well. (d) Cytoplasm of that part of the PC outlined in "C" that contains numerous mitochondria (m) and a distinct Golgi apparatus (g). (e). The PC pole (green) delineated in the low part of "C" is composed of in- and out-folds that interdigitate with the distal process of another presumptive PC (coursed by dots). (f) 3D view of 25 sections through the outer aspect of PC karyoplasm. Scale bars = 1 μm in (a) and (c), 0.5 μm in (b), (d), (e), O.2 μm in (g).

originating from the parent CBV can pierce the neuropil to become associated with the pericyte located in a nearby CBV.

A fourth additional cytoplasmic specialization of the pericyte that was identified in this study consists of a single, stright process termed to as "string process" (Figures 2a, 3a, and 6). The SP is a single, string process leaving the perikaryon from the apex of a funnel-like extension (Figures 2a and 6a,c,e,f) or less frequently from a process (Figures 3a and 6b,d). In the latter instance, the SP shaft may be identified along the cytoplasm of the parent process (Figure 3a). Although an SP varies in length (i.e., 15 to 120 μm), it has a uniform diameter (i.e., 0.3 to 0.5 μm), and a zigzag flexure is observed in more than two-thirds (i.e., 78%) of them (Figure 6a–c,f). Distally, the SP enlarges abruptly to eventually form a vesicular complex composed of either dense, confluent spherules (Figure 6d,e) or delicate membranous outgrowths (Figure 6b,c,f). The overall area occupied by these complexes is variable and may be as large as 5 μm on the longest axis. Because we could not find any prior descriptions of this type of membranous structure, the term terminal vesicular complex is suggested.

### 3.1.2 | Tangential interactions: Perforating SPs

Although the association of interlacing pericytes (Figure 3b) paralleling the CBV wall is implicit, a set of SPs allows for the capillary domain to reach processes of a homologous cell that is in a nearby (i.e.,

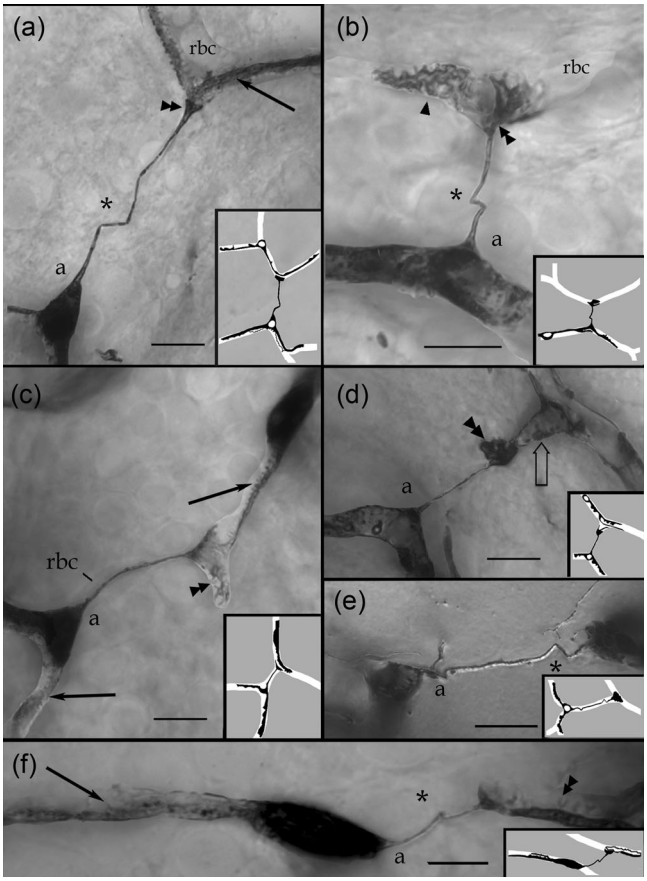


**FIGURE 6** Photomontages of string process-bearing PCs. (a) Two CBVs outlined by the PC perikaryon (lower left) and primary processes (upper right, arrow). Notice that the former extends a perforating string process devoid of an associated CBV. Also Notice that the SP zigzags (*) at the middle to end into a triangular vesicular complex (double arrowhead), which appose with the primary process (arrow). (b) Another perforating SP bridging two CBVs. The SP (a) resolves in a membranous extension (double arrowhead) next to a secondary process (arrow head) associated with the CBV in the upper part (not shown). rbc = ghost of a red blood cell. (c) Two PCs with overlapping, distal processes. Arrows = secondary process, double arrowheads = membranous extension of the SP (a) riding in an unstained CBV. rbc = ghost of a red blood cell. (d) A perforating SP (a) creating a dark-bizarre ending (double arrowhead) next to a mesh process (hollow arrow). (e) A PC perikaryon extends an axonid (a) originating as a terminal bouton (double arrowhead). Phase-contrast optics. (f) A bipolar pericapillary PC with perforating SP (a) that resolves next to a secondary process (double arrowhead) in a nearby blood vessel. Arrow = secondary process. The axon appears to terminate at the tip of the dendrite. Double arrowhead = membranous axonal appendage. Scale bars = 3 μm.

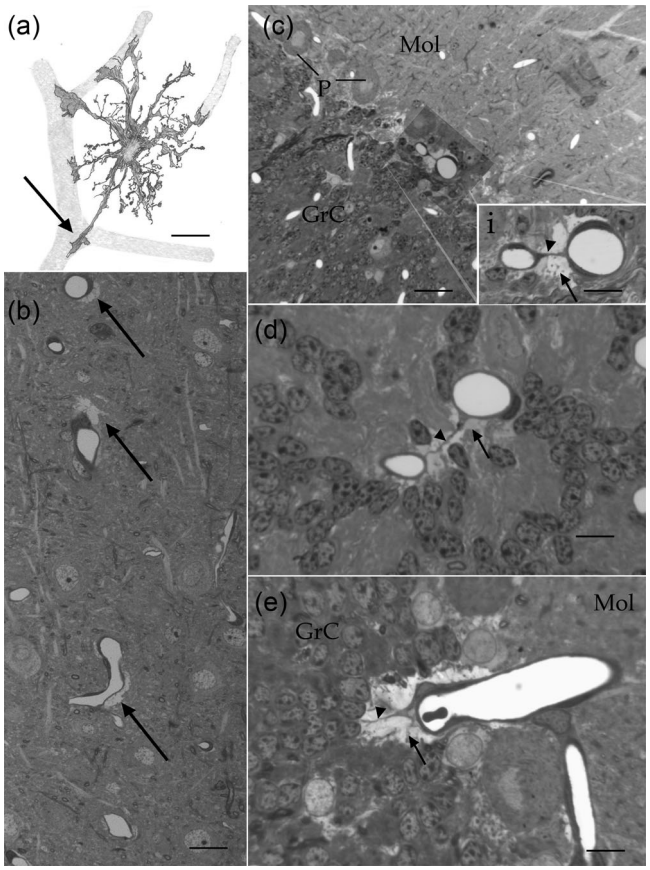


**FIGURE 7** Light microscopic images illustrating the astrocyte and its processes. (a) Camera lucida drawing of a protoplasmic astrocyte creating radial processes that terminate into a flat end-feet (EF) (arrow) surrounding the adjacent CBVs (soft pencil). (b) Semi-thin section showing the patch-like appearance of EF (arrows), which are firmly opposed to CBVs. Parietal cortex, toluidine-blue stain. (c) Micrograph at the intersection of the molecular (Mol) and inner granular (GrC) layers of the cerebellar cortex; between these layers, there is the row of large Purkinje cells (p). Note the two CBVs (shaded) of a first observation of dissimilar diameter. (i) High-magnification of the CBVs in "C" depicting a perforating string process (arrowhead) embedded by EF (arrow). (d) High-magnification micrograph of the cerebellar granule cell layer. (e) A tangential section through a CBV surrounded by a crescent-like structure of EF (arrow). A putative PC bridge can be seen (arrowhead). Scale bars = 10 μm in (a) to (d); 5 μm in "i." Rapid Golgi in "A"; toluidine blue in (c) to (e). Adult rabbit brain. Scale bars = 5 μm in (a), (c)–(e), 10 μm in (b), 3 μm in (i).

different) CBV (Figures 2a and 6a,b,d,f). These perforating processes have been previously described in the cerebellum (Zimmermann, 1923) and retina (Williamson et al., 1980) and are described and found in available series of the human cerebral cortex (Shapson-Coe et al., 2021). Currently, the ubiquity of perforating SP through forebrain CBVs is evident. Hence, pericytes exhibit two different arrangements; specifically, there is a lineal or string arrangement, whereby a pericyte interlaces with its homolog in the same CBV, and a transverse or tangential arrangement, whereby a pericyte originates perforating SP wrap processes of a pericyte of a different CBVs. Further inspection of the CBV back and forth to the tributary penetrating arteriole and vein, respectively, demonstrated that perforating SPs link pericyte-CBVs of a heretofore unsuspected asymmetric caliber (Figure 7c,d). Another thus far neglected feature of perforating SPs is the uninterrupted EF envelope that they exhibit (Figure 7c–d). Observations at the electron microscopy level first confirmed that intercapillary SPs bridges arise from pericytes located in CBVs of different diameters (Figure 8a). Additionally, the pericyte process forms a core in the bridge that is

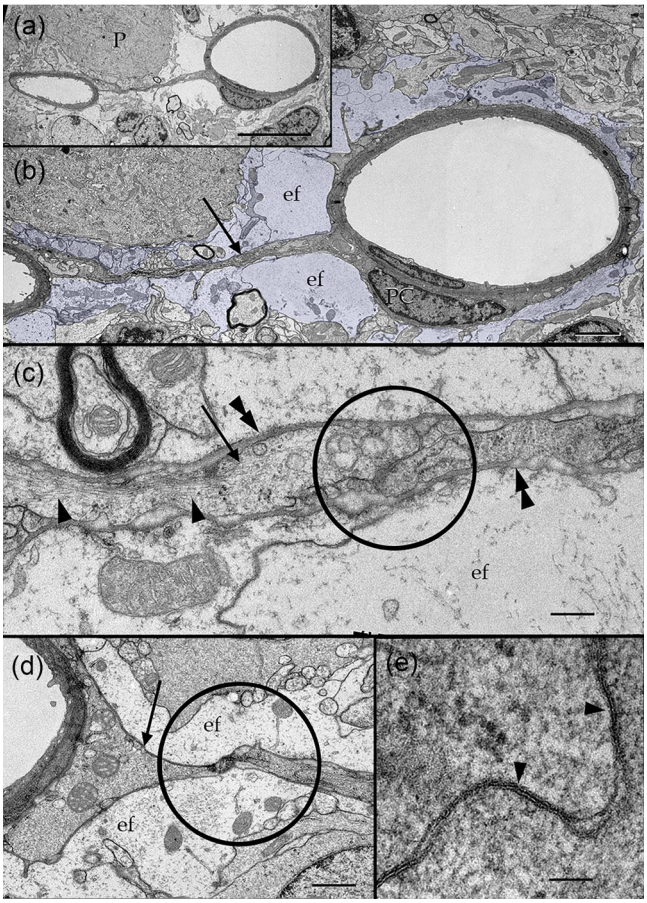


**FIGURE 8** Ultrastructural appearance of the PC intercapillary bridges (ICBs). (a) Low magnification view of an ICB between two CBVs. Note that there is a first-sight asymmetry in vessel caliber. P = Purkinje cell. (b) High-magnification micrograph from the ICB shown in "A." Note the complete cytoplasmic cuff (light blue) that end-feet (ef) paved around both CBV and PC processes (arrow). pc = cell nucleus of a PC. (c) Interaction (circle) between two PC processes (arrows) creating the core of an ICB in the frontal cerebral cortex. Double arrowheads = BL; single arrowheads = microfilament bundles. (d) Contact processes (circle) from two PCs structuring the core of an ICB. (e) High-magnification view of two uniting PC processes. Note that the plasma membrane processes alternate with the zonula occludens (arrow heads). Scale bars = 3 μm in (a), 1 μm in (b), 0.5 μm in (c) and (d), 0.2 μm in (e).

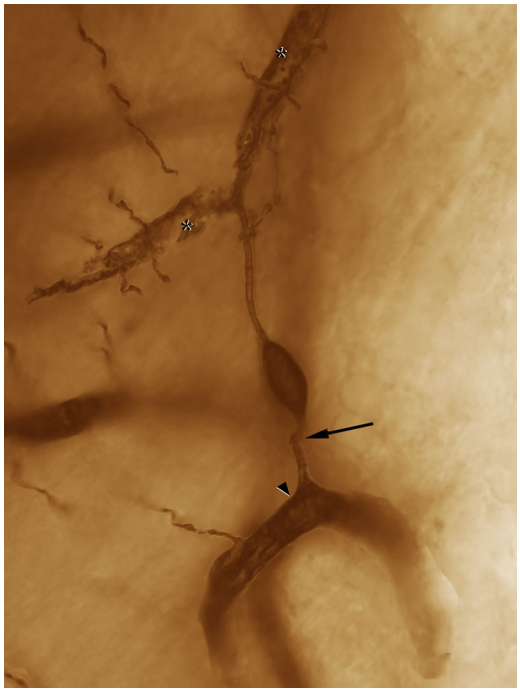

**FIGURE 9** Photomontage of an extracapillary PC. This bipolar PC, which is surrounded by the neuropil sends an ascending, ramifying processes that give rise to typical secondary processes (*) entangling a CBV. The opposite pole of the perikaryon extends a distinct string process anchoring in another nearby CBV (arrowhead). Note the discreet flexure (arrow) of the sp next to the perikaryon. Scale bar = 5 μm.

covered by an EF cuff (Figures 7c,d and 8a–c). Moreover, within the core, convergent processes may entangle each other; in addition, plasma membranes along this cell-to-cell interaction appear to be united by a series of tight junctions (Figure 8c–e), in a similar fashion to that described for the pericyte perisomatic aspect (Figure 5g).

Another outstanding observation is that the pericyte perikaryon and its proximal process may be devoid of a CBV (Figure 9). This uncommon extracapillary location prompts the idea that it corresponds to a neuron rather than a pericyte. However, one of the distal processes usually anchors and surrounds a CBV exhibiting the typical location and structure of a process. Further, the pericyte process leaving the opposite pole of the perikaryon is indistinguishable from a typical SP (Figure 9). To date, only five extracapillary pericytes of this type have been observed (three pericytes in the cerebellar granule cell layer and two pericytes in the cerebral isocortex).

APs, neuron-processes, EF, and perivascular ground substance provide for a seemingly distinct organ. Another frequent membranous appendage of the pericyte is that resulting from paired uneven branches or APs (Figures 2A and 10). A direct search for the APs in various brain areas demonstrated their ubiquity and added structural features, which we summarized in the next few sentences (Figure 10). First, an AP results from the dichotomous division of a primary process into two different branches, known as alpha (αB) and beta (βB) branches. The resulting horseshoe arrangement outlines the CBV contour (Figures 10a–c, hollowarrow), wherein it is wider at sites of ramification (Figures 2a and 10e, **). The αB shaft is intensely stained with silver and measures 1 to 2 μm in diameter, although its length is highly variable (measuring 20 μm or more). The αB is notable due to its four to seven thin, mantle-like, outgrowths comprising the AP concavity. These distinct formations provide the αB an overall appearance of a shelf with assorted membranous extensions on it (Figures 3a and 10). Moreover, the βB is thinner, shorter, and darker than the αB, ranging from 0.5 to 1.0 μm in diameter and 5 to 15 μm in length. An important landmark for αB identification is the pale, lucid appearance as an extension of the BL filling up the AP concavity (Figure 10). Specimens from various mammals demonstrated the

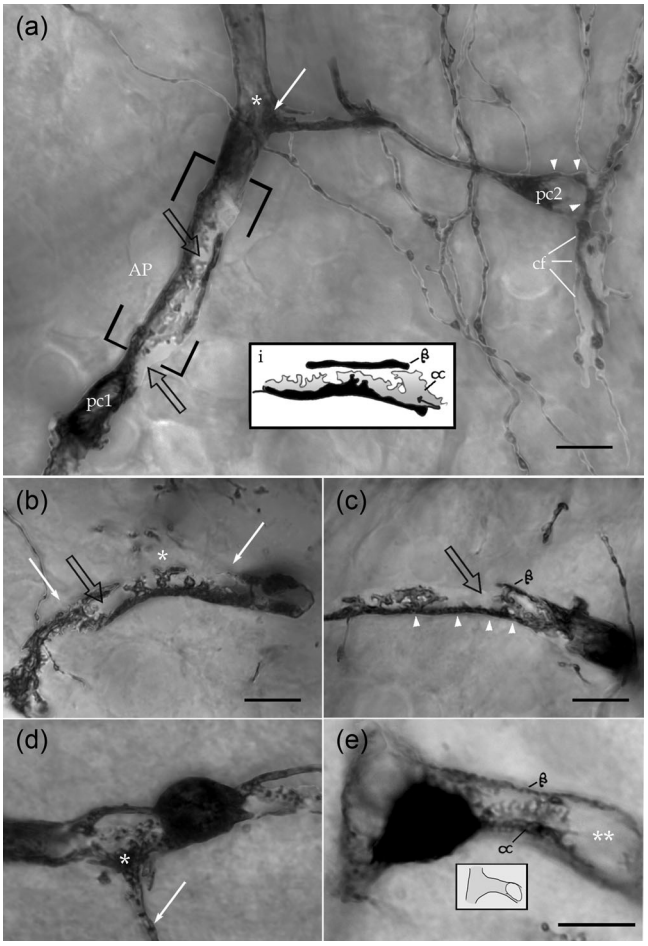


**FIGURE 10** Membranous specializations of the PCs. (a). Anastomosing (arrow) capillaries surrounded by two PCs in the rat cerebral cortex. One of them (pc1) extends a primary process originating an AP. The irregular membranous outgrowths arising from the thicker, or alpha arm ($\alpha$) toward the shorter, thinner, or beta arm ($\beta$) are evident. Note the diaphanous BL (hollow arrows) embedding the outgrowths of the alpha arm. Another perikaryon (pc2) sends a horizontal string process whose terminal vesicular complex (arrow) overlaps the distal process (*) of pc1. cf = climbing fiber encircling (arrowheads) the perikaryon and proximal processes of the pc1. (i). Camera lucida drawing showing the asymmetry between the alpha ($\alpha$) and beta ($\beta$) processes organizing the AP shown in "A" with outgrowths of the alpha branch occupying the recess between the two branches. (b) An AP (between arrows) surrounding an unstained CBV and an emerging branch (*). Hamster posterior thalamus. (c) A long AP in a CBV of the rabbit frontal cerebral cortex. Note both here and in "A" and "B" that there is a pale, chromophobic area (arrowheads) embedding the membranous outgrowths from the thick argentaffin, alpha processes, which oppose to the beta ($\beta$) process. (d). Specimen of the mouse cerebral cortex showing the perikaryon of a PC bounded by two APs. Note that the arriving terminal vesicular complex (*) of a penetrating string process to the AP domain. Arrow = string process. Cerebral cortex. Perikaryon surrounding a CBV ramification. Note that the cell gives rise to an AP along the capillary shaft (right). (e) Rhesus monkey frontal cortex of a PC with proximal processes that organize an AP that distally encircles an arising CBV (*, **). Calibration bars = 5 µm.

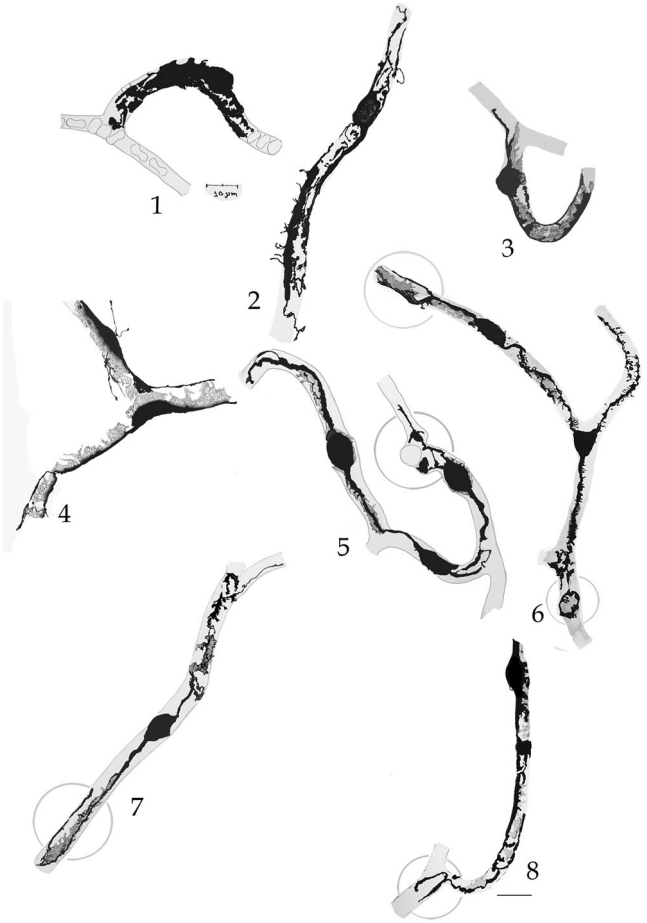


**FIGURE 11** Camera lucida drawings of the PC in CBVs of various mammals. Human (cells 1 and 2), rhesus monkey (cell 3); cat (cell 4), guinea pig (cell 5), rabbit (cell 6), mouse (7), and rat (8). Circle = mesh process. Cerebral cortex, rapid-Golgi technique. Calibration bar 5 µm.

conservation of pericytes in mouse, albino rat, guinea pig, kitten, rabbit, rhesus monkey, and human brain samples (Figure 11). Under the electron microscope (Figure 12), the $\alpha$B-AP lies underneath the EF, and its $\beta$B is located just outside of the oBL, thereby paralleling the CBV lumen (Figure 3b). Moreover, serial sections and 3D reconstruction at the root of a CBV provide further characteristics of the AP. The first characteristic includes the fine structure of the BL comprising the $\alpha$B concavity. This structure consists of a 2-fold BL (Figure 12d,e); specifically, there is a sharp layer of moderate to high electron density, or *pars densa*, associated with the $\beta$B, and an electron-diaphanous one, or *pars lucida*, surrounding the membranous outgrowths of the $\alpha$B. An additional distinct feature of the *pars lucida* is that its homogeneous matrix is traversed by numerous strands from 15- to 18-nm thick that extend radially between $\alpha$B and $\beta$B inner aspects (Figure 12e), thus mimicking those strands embedded in the Pacinian corpuscle BL (Dubovy & Bednarova, 1999; Munger et al., 1988). 3D reconstructions of the $\alpha$B and $\beta$B (Figure 12b,c) demonstrated the unique interaction between these structures. Tiny, inconspicuous axons piercing the EF observed in single sections (Figure 12a, arrows) correspond to a set

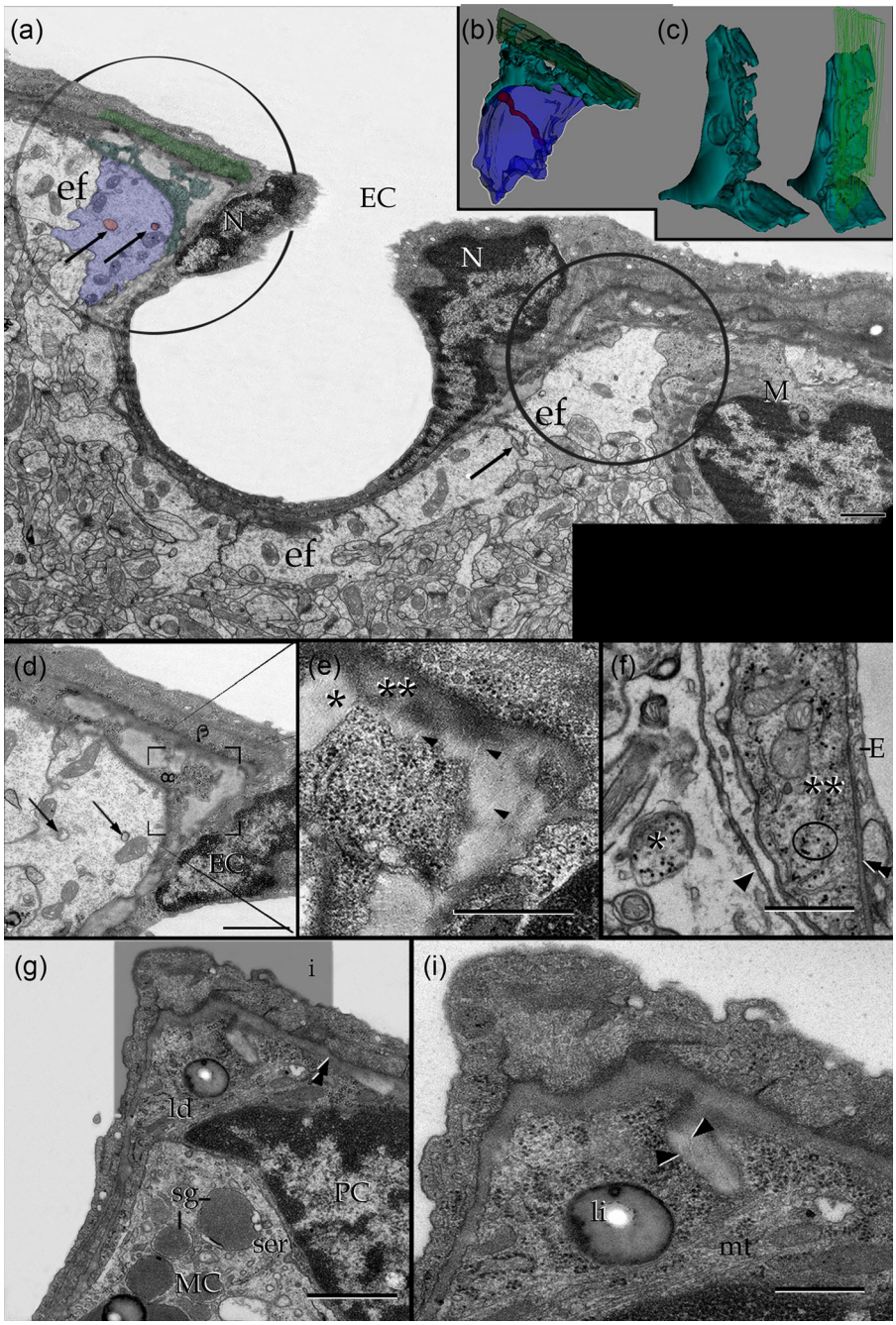


**FIGURE 12** Electron microscopic micrographs of the capillary neurovascular unit in 2D and 3D images. (a) Survey micrograph at the site of origin of a transversely sectioned CBV. The AP (green) consists of paired ($\alpha$ and $\beta$) branches (arrows). Due to the annular shape of both the endothelial cell nucleus (N) and the AP proper (circles), they can be observed twice on either side of the capillary root. Astrocytic end-feet (ef), and a nearby microglia (M) provide continuous coverage to the AP. Note that the end-foot (blue) covering the AP proper is pierced by a thin nerve (red, arrows) or GCE. (b) Reconstruction of 55 consecutive sections through the portion of the AP encircled in "A," left side. The external structure of the asymmetrical, opposing $\alpha$ (turquois) and $\beta$ (green-colored) arms of the AP is evident (see Figures 2 and 10). Note that the outer aspect of the AP is covered by the endfoot (blue) that is correspondingly traversed by the GCE (red) creating a distinct enlargement next to the AP. (c) Appearance of that part of the $\alpha$ component (left) of the mesh processes facing the $\beta$ outgrowth that appears outlined in light green (right). (d) Micrograph through the opposing alpha ($\alpha$) and beta ($\beta$) arms of the AP process reconstructed in "B and C." The stem nerve originating from the GCE reconstructed in "B" can be observed (arrows). (e) High-magnification micrograph from that part of the field labeled in "D." Note the BL embedding the AP exhibiting two, distinct constituents: a thick, electron-opaque, component (**) or pars densa and an electron-diaphanous or pars lucida (*), the latter structure is pierced by light, radial threads (arrowheads). (f) Section through the wall of CBV with endothelium (e) that covers a PC process (**) containing abundant electron-opaque glycogen particles (circle), as well as mitochondrial and sparse rough endoplasmic reticulum. Single arrowhead: outer capillary BL; double arrowhead = inner capillary BL. (g) A section through an endothelial cushion protruding to the lumen of a CBV. Underneath the

*(Continues)*

**FIGURE 12** (Continued)
inner capillary BL (double arrowhead), there are portions of a PC with cytoplasm that contains numerous free ribosomes, scarce rough endoplasmic reticulum, and a solitary granule with lipid droplet material (li). Next to the latter, there is the weakly electron-dense cytoplasm of a perithelial fluorescent cell (MC), containing large, rounded, secretory granules (sg) surrounded by cisternae of the smooth endoplasmic reticulum (ser), and rough endoplasmic reticulum. (i) High-magnification view depicting an invagination containing the electron-lucid BL associated with an AP as confirmed by identification through the adjacent sections. Note the presence of light, radial fibrils (arrowhead) embedded in the pars lucida bounded by the invagination itself. mt = microtubules. Calibration bars = 1 μm.

of synaptic outgrowths termed here GCE reveled by 3D reconstructs (Figure 12b,c).

A singular feature of the AP is its frequent association with the endothelial cell, end-foot, and Mato cell; however, in no case are these interactions direct because the iBL and oBL interpose (Figure 12e,g(i)) between them. A distinct set of nerves arising from the perivascular neuropil invaginate through the EF to settle on that portion of it that overlays the AP proper (Figure 12a,b). Due to the long shaft end, dilatation of these nerves signifies the abovementioned GCEs. The source and fine structure of GCE and its interactions with the CBV will be the core subject of the following paragraphs. However, before proceeding with the description of the pericapillary neuropil, it is necessary to highlight the structure of the second cell type that is associated with the capillary wall.

## 3.2 | Mato cell

The ubiquitous perithelial fluorescent cell paraformaldehyde (PFC) (Mato et al., 1980, 1984), also known as the granular pericyte (Mato et al., 1996) or later referred to as type II mast cell (Dimitriadou et al., 1987; M. -F. Yang et al., 1996), share an intermembranal position between the iBL and oBL (Figures 13 and 14; Graeber & Streit, 1990). Due to this, both cell types are an integral part of the neurovascular unit (NVU) (N. Li et al., 2017; Ribatti, 2015). Thus, the rounded PFC soma lies next to CBVs (Figures 12G and 14), usually at sites of ramification (Figure 13a), detected in decreasing frequency in the thalamus, basal ganglia, olfactory bulb, hippocampus, and isocortex. The perikaryal PFC contains an oval nucleus surrounded by numerous granules larger than 1 μm thus providing an overall foamy appearance to the cell. Like a pericyte, the Mato cell sends long paired cytoplasmic processes alongside the CBV wall. Unlike the former type of cell, PFC processes may be exceedingly thin (Figure 10a) and equally longer than 100 μm. Additionally, the presence of solitary granules surrounded by the same organelles contained by the perikaryon (Figure 13) was observed to secure the identification of distal PFC processes (Figure 10e,f). Another cytoplasmic landmark of the PFC is the large area occupied by the smooth endoplasmic reticulum surrounded by anastomosing granules (Figures 13A and 14), which has a limiting membrane that is reinforced by a fussy material. A set of the later granules that are scattered next to the plasma membrane contains distinct electron-diaphanous material that is seemingly identical to the collagen fibrils scattered in the BL (Figure 14). The identification of continuity between cytoplasmic granule contents and extracellular collagen fibrils (Starborg et al., 2008) in series (Figure 14) provides an emerging notion favoring the role of PFC in BL synthesis.

## 3.3 | End-feet and pericapillary tripartite synapses

Although a few uncommon extensions of EF penetrate between the oBL-iBL domain, EF rests on the oBL alternating with occasional microglia (Graeber & Streit, 1990) or scattered throughout the neuropil (Varela-Echevarría et al., 2017). Because the contribution of microglia to the pericapillary structures described in this study is absent or occasional (Figure 12a), microglial cells will not be considered in this article. The EF mediates between the pericapillary neuropil and CBV proper. The abluminal surface of the CBV is partially covered (Figures 5a,c and 15a; Bertossi et al., 1997) by a set of EFs (Figures 2b, 7a, and 12a), which adapt to the capillary wall and adjoining neuropil in an inseparable fashion (Figures 15–18). Under the light microscope, the EF consists of a pale, chromophobic enlargement of a parent process encasing the capillary wall. Generally, perivascular EF location is the most common; however, a set extends from the CBV wall to cover the intercapillary bridges of the pericyte, which has a core consisting of presumptive SP (Figures 7c–e and 8a–c). In either case, the EF–SP interaction is indirect because the oBL interposes between them (Figure 8c,d). As shown in Figure 15, each EF covering the cortical or thalamic CBV wall displays at least three distinctive portions. The first portion is highly convoluted or convex, whereby the EF directly interacts with the surrounding neuropil. This part is continuous with the EF pedicle (Figures 2b and 7a). A second, or inner part (i.e., capillary) is smooth and concave as it outlines the oBL. The third portion is a lateral, interdigitating that part eciprocates that of the neighboring EF that defines distinct gap junctions (Figure 15b; Bertossi et al., 1997). Overall, EF differs from both the neuropil and CBV proper by their low electron-lucid cytoplasm possessing a paucity of organelles although distinct clusters of mitochondria and smooth and rough endoplasmic reticulum may be observed next to the oBL (Figures 15c and 17d,e). Other than the latter part of the EF cytoplasm, we could not identify the florid collections of secretory organelles described elsewhere (see Boulay et al., 2017). Moreover, a defining feature of the EF is that it is virtually devoid of bundles of intermediate filaments that otherwise may easily be observed in the cytoplasm of the perikaryal or paraxial, proximal processes (Hama et al., 1994; Varela-Echevarría et al., 2017). An additional, distinct characteristic of EF is that its plasma membrane defines a continuous envelope to the intended nerves that interact with the capillary wall (Figures 15e,f,i and 16a,e–g). To emphasize, once a prospective pericapillary nerve approaches the parenchymal convexity of the EF, it proceeds toward the capillary BL that is engulfed by the cell membrane of the later structure; hence, when the penetrating nerve reaches the oBL, the inner and outer EF cell membranes interpose between

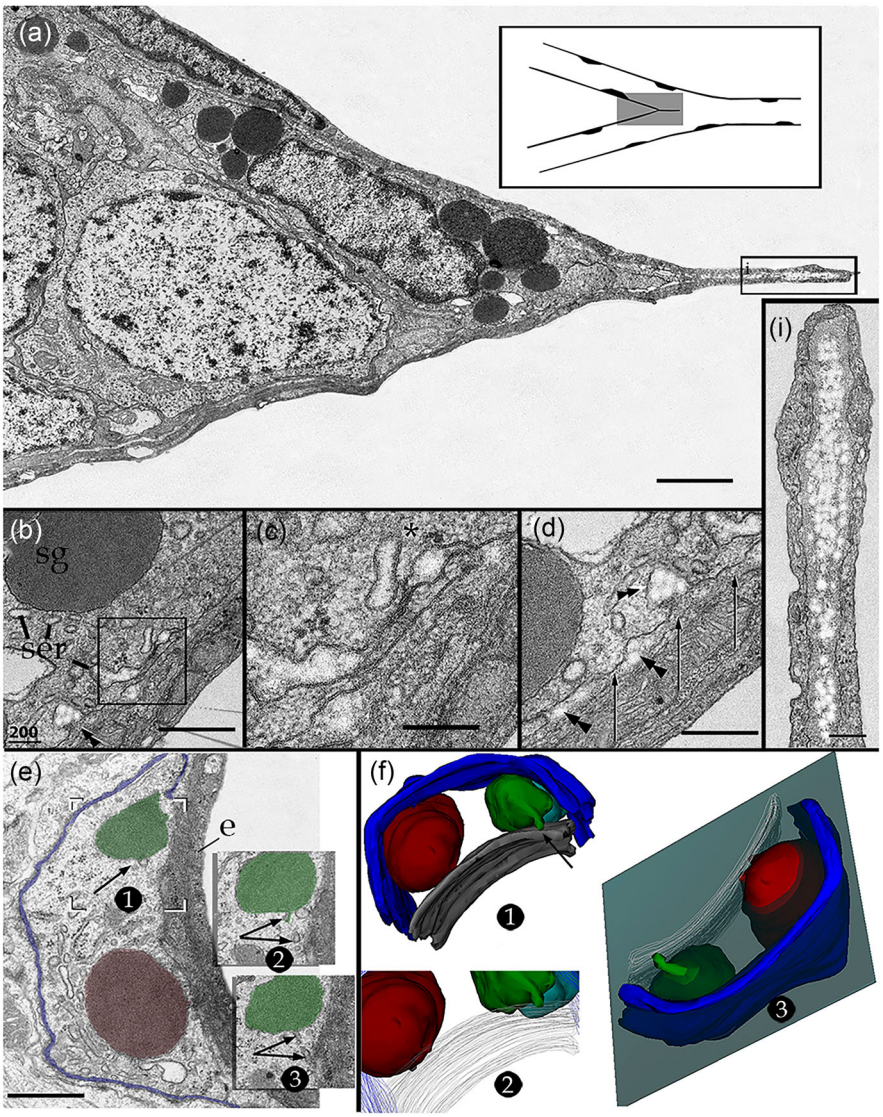


**FIGURE 13** Bi- and 3-D electron microscopy of perithelial fluorescent cells (PFCs). (a) A PFC at the mesangium of a forked CBV that contains numerous electron-dense, secretory granules (sg) scattered in the cytoplasm. An endothelial shaft protruding from the mesangium to the lumen can be observed. (i) High-magnification view depicting the core of the shaft containing electron-lucid clusters of collagen fibrils. (b) Micrograph of the interaction of the PFC cytoplasm with the extracellular matrix; note the anastomotic tubes of the smooth endoplasmic reticulum (ser), containing electron-lucid material. Extrusion of the electron-lucid material to the endothelial BL (double arrowhead) may also be observed. (c) High-magnification view of the area outlined in "B" whereby the appearance of ser content is further appreciated. (d) Micrograph contiguous to clusters of collagen fibrils partially encircled by the smooth endoplasmic reticulum (upper right) or embedded (arrowheads) in the endothelial inner BL (arrows). (e) Series throughout distal processes of the PFC. In micrographs 1 to 3, a tiny duct (arrow) between the secretory granule (green) and extracellular matrix is shown. (f) 3-D views of the series shown in "E." 1. Upper view of secretory granules. 1. and 2. The continuity of the narrow tube (arrow) with the secretory granule (green) and endothelial BL (gray) is evident. Blue = external BL. 3. Similar to the perikaryon (b to d), the process of the PFC is encased by a continuous BL formed by the endothelial (gray) and external (blue) capillary BLs. Calibration bars = 1 μm in (a); 0.5 in (b)–(e); 0.2 in (i).

them (Figure 17a,b). Alternatively, pericapillary nerves also approach the oBL *between* two EFs and remain sequestered, thereby preventing direct contact with the oBL. Aside from either modality of the EF envelope, nerve processes do not contact the oBL (Figure 17a–d). Another novel EF characteristic occurs in its vascular aspect. Specifically, there are one or two long invaginations (Figure 15d,e) left by a longitudinal outgrowth of the oBL, which is described in the following accounts. Specifically, the EF surface exhibits the impressions left by penetrating elements at the superficial and deep facets of this structure (Figure 15d,f).

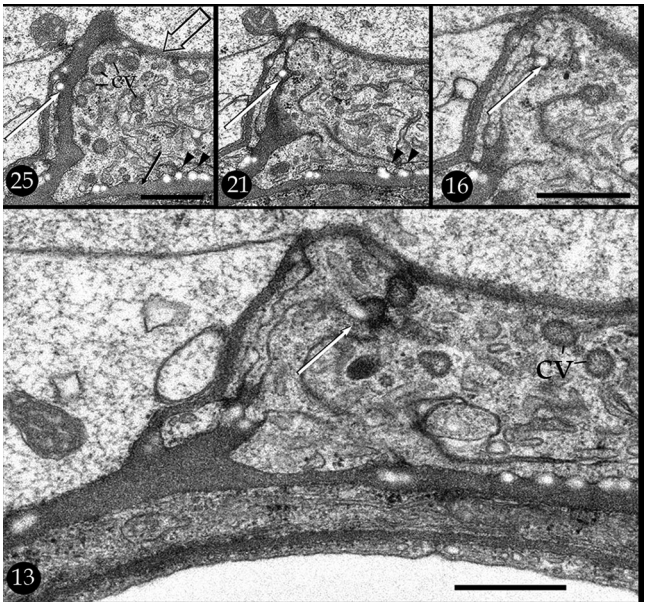


**FIGURE 14** Semiserial sections (Arabic numbers) of the juxta-nuclear cytoplasm of a Mato cell. Note in Section 25 that the later structure lies between the inner (black arrow) and outer (hollow arrow) BLs, which embed clusters of cross-sectioned collagen fibers (arrowheads). The series shows the progression of a collagen fibril (white arrow) from being embedded in the outer BL (white arrow) (Sections 25 and 21) to appearing invaginated (Section 16) after which it progresses to the lumen of the secretory vesicle, (white arrow, Section 13). cv = coated vesicles. Scale bars = 0.5 μm.

## 3.4 | GCE

Among the broad category of pericapillary nerves, GCEs are the most frequently observed in thalamic and neocortical specimens. A typical GCE arises from an axo-dendritic synaptic contact that otherwise matches an axo-dendritic chemical synapse in every respect (Peters et al., 1976), thus defining a modified TS (Araque et al., 1999). Unlike a typical TS surrounded by a peripheral astrocytic process, 3D reconstructions of pericapillary TS, which are usually axo-dendritic, are surrounded by the EF proper (Varela-Echevarría et al., 2017). The minute and variable dimensions of a GCE (i.e., 0.3 to 5 μm in length and 0.2 μm in diameter) require reconstructions of series to be fully visualized. A typical GCE consists of a funnel-like out-growth descending for a variable distance in the direction of the oBL (see above), after which it opens into the enlarged, end-sac part of the GCE (Figures 15e,f,h,j, 16g–i, and 17a–c). Vesicular contents of the parent bouton and the arising GCE include numerous small, agranular vesicles that, together with a dendritic spine or shaft (Figures 15E,H and 16A), define an asymmetrical synaptic contact (Peters et al., 1976). Both the stem and the end sac of the GCE also contain scattered rounded synaptic vesicles (Figure 17a,b) with scarce rounded electron-dense core vesicles (Figure 17b). GCEs containing flat, pleomorphic vesicles are uncommon (Figure 18f), averaging two for every 50 GCEs. Careful observations of the GCE cytoplasm have failed to identify active zone(s) and/or junctional complexes other than that of the parent bouton. Although there is a neighboring, putative effector structure of the GCE, clusters of synaptic vesicles appear to be polarized toward the oBL (Figure 17b,d). Due to the abovementioned GCE engulfment by the EF, the interposed inner and outer cell membranes lie squeezed between the former structure and the oBL (Figure 17a–c). Furthermore, GCEs are ubiquitous throughout central CBVs, and we have additionally identified them in series from the olfactory bulb and peduncle (data not shown). The outstanding GCE structure is commonly shared by the interstitial ground substance as commented upon in the next section.

## 3.5 | Interstitial ground substance

In addition to the oBL specializations described for the pericyte-AP, there is still another previously unnoticed structure in CBVs throughout the forebrain. Transverse sections through the CBVs exhibit two to five small outgrowths of the abluminal aspect of the oBL, which matches the longitudinal concavity described for the EF (Figure 15d). This type of outgrowth, which is referred to in this study as the LC, approximates 0.5 to 2.0 μm in height by 0.3 μm in width (Figures 16a–f and 17). Furthermore, sections paralleling the CBV longitudinal axis demonstrated that the LC extends along the entire CBV length (Figure 18). Although the LC is a homogeneous extension of the oBL matrix, clusters of one to four collagen fibers may be observed as being embedded in approximately one-third of them (Figure 16a,b). The shape and dimensions of the LC are uniform throughout the brain CBVs but are variable in the cerebellar cortex (see below). Moreover, the LC association with the terminal expansion of the GCE appears to be a fundamental site for neurovascular interaction (Figures 16a–f and 17b–d). Direct interactions of the GCE with areas of the oBL devoid of LC were uncommon in samples from the thalamus and isocortex (Figures 16g,i).

At the stage of our description, it is advisable to return our attention to Figure 16. The dendritic shaft (d) of a thalamic neuron receives a series of consecutive boutons whereby it sends each a single GCE that anchors in the same order along the LC as defined by reconstruction of the series. The peculiar sequence of synaptic bouton-GCE-LC was also observed in the cerebral isocortex (Figure 18c), and the basal ganglia (data not shown) may suggest ubiquity. Figure 19 summarizes these descriptions and shows the neuro-glial capillary unit (NCU) as a whole. The emerging question about the possible source(s) of prospective pericapillary dendrites receiving synaptic bouton-GCE-LC should be initially approached in Golgi-processed specimens.

A set of distal dendrites from cortical pyramidal (Figure 20), medium size spiny (Somogyi & Smith, 1979), thalamic projecting (Clascá et al., 2012) (Figure 21) cerebellar and cerebellar granule and Purkinje cells undergoes structural modifications at their respective vascular intersections. In general, pericapillary dendrites are enmeshed in glial processes. The structural modifications of pericapillary dendrites proper may be summarized as follows: first, one to four balloon-like enlargements of the parent dendritic shaft resulted in a tuberose appearance (Figures 21a,b and 22e). These rounded outgrowths expand and produce assorted membranous appendages of variable length. A third

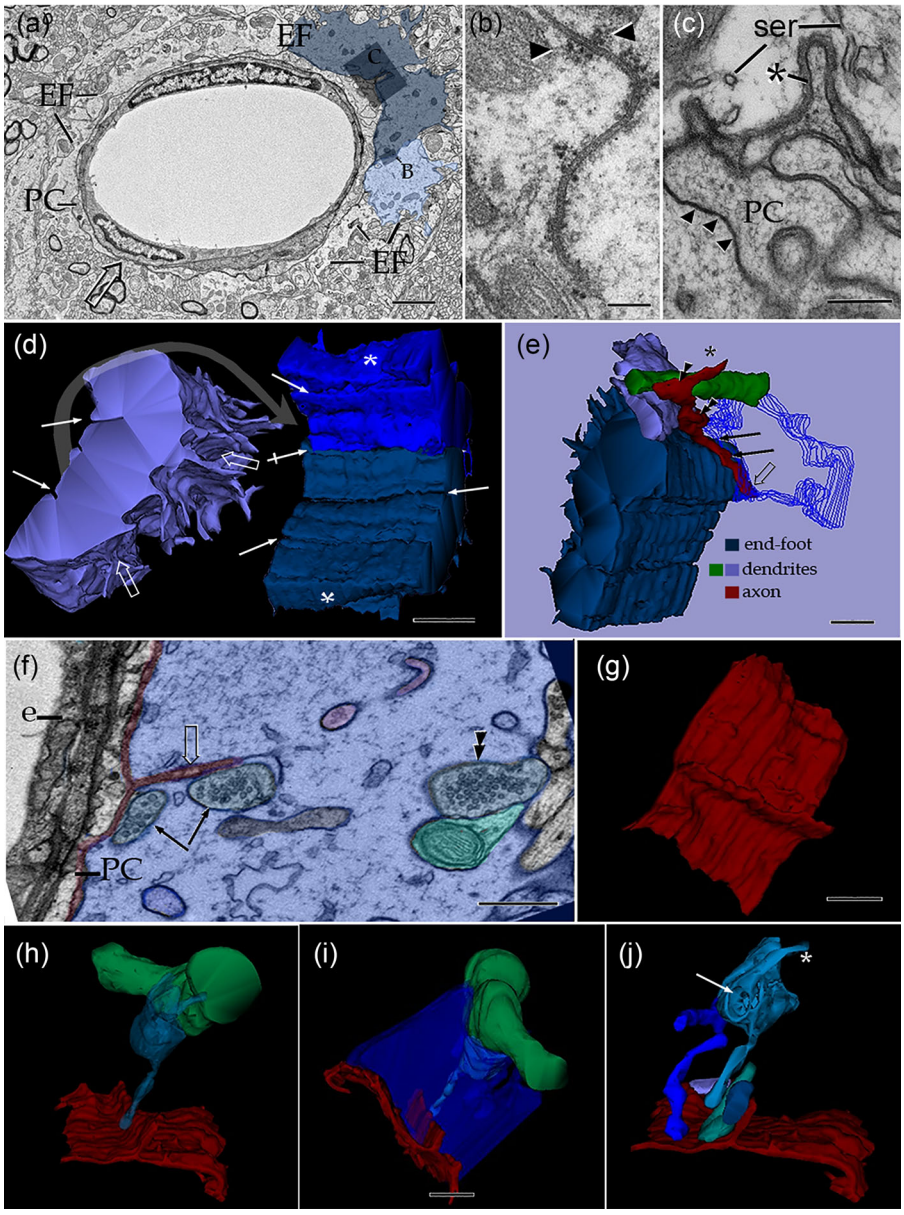


**FIGURE 15** Electron microscopic inner structure and external appearance of glial and neural specializations of the pericapillary domain. (a) Survey micrograph of a CBV in the cerebral cortex from the same specimen as that shown in Figure 7b, upper arrow. Notice the discontinuous (hollow arrow) mantle of astrocytic end-feet (EF) built up between the capillary wall and the neighboring neuropil. Two endfeet shaded in pale blue are featured in panel figures "D" and "E." (b) Intersection of two endfeet sealed by a long gap junction and clusters of glycogen particles (arrowheads). (c) A LC; * of the external BL. Underneath there are interlacing PC processes protruding to the LC and united by tight junctions (arrowheads). (c) High-magnification view of two presumptive interlacing processes (PCs) bounded by the outer BL. * = LCs containing protruding processes. Arrowheads = tight junctions between processes. ser = smooth endoplasmic reticulum. (d). 3D reconstruction from 150 sections. The elaborate, convoluted parenchymal surface (left, hollow arrows) of the end-foot contrasts with the concave, smooth appearance of the inner, stromal aspect (right) of the adjacent end-feet showing longitudinal sulci (white arrows) that the LC can imprint. * = lateral aspect of the endfeet. (e) Complete (dark blue) and incomplete (outlined in light blue) reconstruction of the endfeet shown in "D" to disclose the neural processes between them. An arriving axon (*) gives rise to a modified tripartite synapse (TS; double arrowheads). The axon fibril (*) gives rise first to two synaptic boutons terminating in their respective dendritic tributaries (green and purple colored). Afterward, one of them (double arrowhead) gives rise to a descending (arrows) GCE running toward the capillary wall to end into a discreet enlargement (hollow arrow) next to the oBL (not shown). Notice that both the dendritic and axonal components of this complex lie wrapped by the lateral aspects of the two endfeet. (f) Electron micrograph from a section of the series reconstructed in successive panels (i.e., g to j). The end-foot (blue) resting in the oBL (red) partially and completely embeds a dendrite (green) and various enlarged GCEs (assorted colors). The parent synaptic terminal (double arrowheads) contacts the dendritic spine (green) and gives rise to the GCE (arrows) anchoring next to the outer BL (red) and the ensuing LC (hollow arrow).

*(Continues)*

**FIGURE 15** (Continued)
e = endothelium, PC = pericyte. (g) Outer aspect of the complex BL-LC facing the overlaying end-foot, as seen in "F" or "I." (h) The synaptic bouton targets a pericapillary dendrite (green) and extends a GCE (both colored in transparent blue) close to the LC. (i) Visualizing of end-foot (deep blue) illustrates its close interaction embedding the neural and interstitial (i.e., BL) elements of the complex. (j) Reconstruction of the five GCE extensions identified in the 4 μm encompassing the entire series. Note that four of them lie close to the LC. * = parent axon; arrow = niche occupied by the spine shown in "F." Scale bars = 0.5 μm in (a), (d)–(j); 0.3 μm in (c); 0.2 μm in (b).

dendritic specialization occurs in the distal dendrites of pyramidal neurons (Figures 20a and 21d) and consists of short and narrow, supernumerary branches they are covered by a few pleiomorphic, atypical spines (Figure 21d). Farther distally, the tributary dendrite(s) resume their former structure. Although most dendritic–CBV interactions occur of passage, few terminal branches end up in the perivascular domain (Figures 21c and 22e). Another distinct feature of the dendrite–CBV interaction is the translucent EF mantle surrounding them (Figures 20a and 21a). Since pericapillary dendritic interactions of the NCU represent an obvious candidate for the GCE-synaptic bouton output (Figure 19), a search for their respective parent neuron and axonal tributaries was subsequently performed.

The previous descriptions focused on short interactions of perivascular nerve processes with glial and interstitial matrix specializations (Figure 17) of the capillary wall. However, it is insufficient to demonstrate the neuron types providing dendritic and axonal extensions to the neuropil-CBV domain. Thus, a search for fine structural interactions with the CBVs in the cerebellar cortex was performed with the combination of the Golgi technique with transmission electron microscopy and 3D reconstructions.

Tributary neurons to the pericapillary neuropil. Inspection of the GCs in the homonymous layer of the cerebellum demonstrated various neuro-vascular specializations (Figures 22 and 23). For instance, occasional, modified GC dendrites entangle the capillary wall to form globular structures attached to fine cytoplasmic bridges (Figure 22b). A dramatic interaction of this type of dendritic–CBV association occurs when a side branch from the dendritic shaft extends a long collateral of large, alternating spherules abutted by thin bridges embedded by the capillary wall (Figure 22e). Although the GC axon ascends unbranched to the molecular layer (Palay & Chan-Palay, 1974; Ramon y Cajal, 1904), our observations depict an additional set of short and long axon collaterals to the CBV. Perhaps the most signature characteristic consists of a very short collateral made up of numerous rows of anastomotic vesicles masking the pericyte processes (Figure 22a,b,d). Electron microscopic observations of dendrites at the GC–CBV interaction demonstrated that some globular structures arising from proximal dendrites are indeed small oval extensions facing the oBL (Figure 23a). 3D ensembles further demonstrated that the indistinct EF (Figures 23c and 24c) provides an uninterrupted envelope to the GC outgrowths (Figure 23c). Although appositions of the GC perikaryon itself with the CBV are uncommon in our sampling, occasional finger-like outgrowths to the CBV wall were observed. As most neuron processes interact with the CBV wall, somatic extensions are encased by the EF (Figure 23d).

fMFs represent one of the chief afferent fiber systems to the cerebellar cortex. The ascending MF is a myelinated axon that alternates with large synaptic complexes or rosettes whose fussy appearance confers its name (Chan & Palay, 1971; Hamory & Somogyi, 1983; Jakab & Hámori, 1988; Ramón y Cajal, 1904). Our observations of the GCE layer revealed the presence of peculiar MF–CBV intersections (Figure 24a). These interactions consist of small rounded-to-oval extrusions of the rosette adjacent to the pericyte processes (Figure 24b). MF–CBV excrescences may be pleomorphic; however, most of them are drumsticks (Figure 25b(2,3)) or small swellings. Occasionally, rosette-CBVs may be partly engulfed by a rosette (Figures 24b(1) and 25A). Moreover, reconstructions of sites of rosettes-CBV appositions (Figure 26) complement light microscopic observations, which showed that as the MF approaches the CBV, it extends an outgrowth and is surrounded by an EF envelope (Figure 26).

Ramón y Cajal (1904) described that blood vessels imprint in the Purkinje cell dendrite areas devoid of spines. These dendrites can be observed in our specimens (Figure 27a). Electron microscopic observations at the Purkinje cell dendrite–CBV intersection demonstrated that a unique neuropil may be located and squeezed in the intersection. This result contrasts with the radial arrangement observed throughout the dendritic tree of this cell type (Lee et al., 2005). Rather than being devoid of spines, pericapillary dendrites exhibit sparse, bent dendrites receiving axo-spinous synapses are engulfed by the EF cytoplasm (Figure 27b,c). The later synaptic terminals match those described by Palay and Chan-Palay (1974); however, the synaptic bouton contacting a dendritic spine exhibited a GCE, and both are embedded by an inconspicuous EF. Unlike most interactions of the GCE-oBL in both the cerebral cortex and thalamus (Figures 15–19), LCs in the cerebellar cortex are sparse (Figure 26B,D) and may be exceedingly (i.e., >3 μm) long (not shown). Like CBVs elsewhere in the forebrain or diencephalon, tight pericyte processes lie between the smooth iBL and oBL (Figures 26b and 27c). Furthermore, Purkinje cell dendritic spines receiving climbing fiber synapses may also be encased by an indistinct EF (Figure 27e–g). No 3D ensembles from these synapses are available.

Located just above the row of Purkinje cells, the basket cell is unique because of its unique axon, entangling its somata (Chan-Palay, 1974). In our sample, the two sets of different axonal branches that had previously been described (Chan-Palay & Palay, 1971; Ramón y Cajal, 1904) were identified (Figure 28a). One of the sets defines thick axon terminals about the Purkinje cell (i.e., baskets). Another type of axon, which is usually represented by beaded fibrils (Palay & Chan-Palay, 1974), commonly arises from the parent thick axon ascending to the pial covering. However, we observed that baskets may additionally branch into occasional beaded axons that ramify profusely encasing CBVs (Figure 28a,c). Serial sections of the intersection of the GC-molecular-layer demonstrated that basket cell axons traveling in the pericapillary

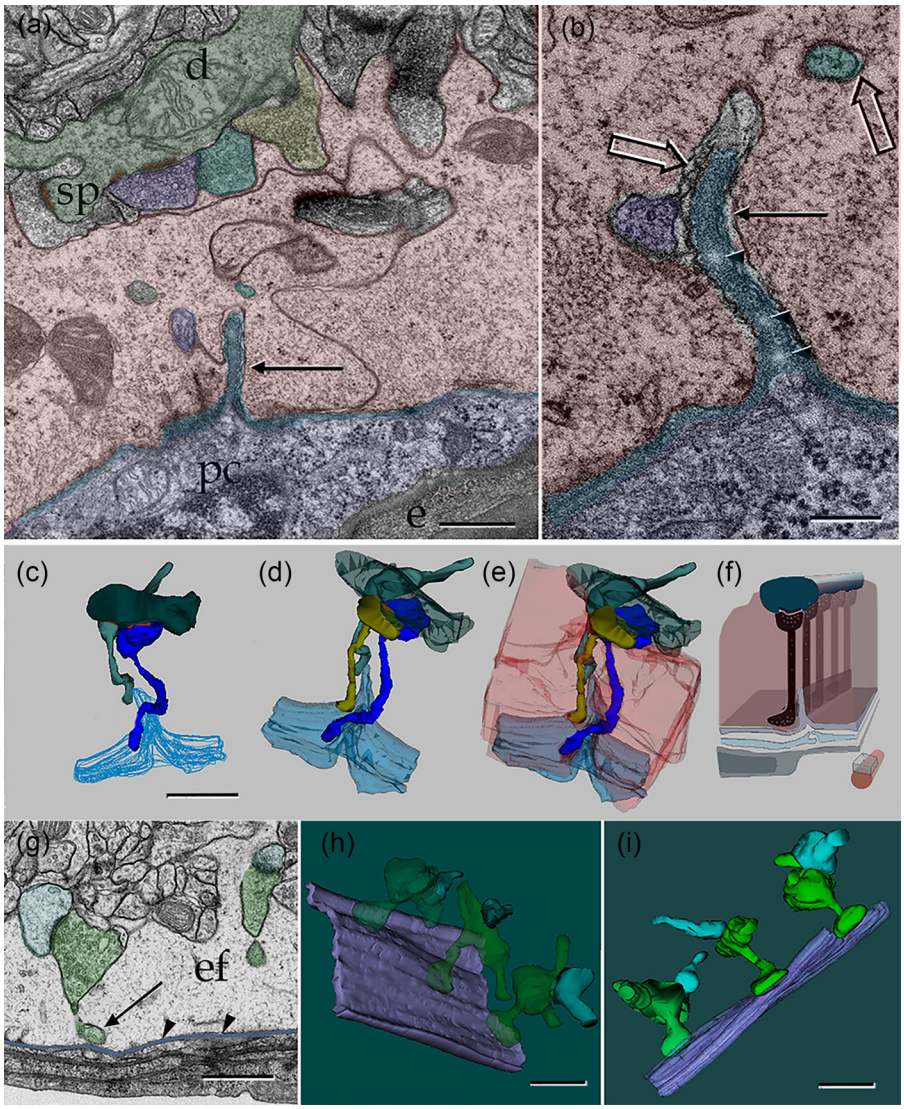


**FIGURE 16** Series through the brain neuroglial capillary unit (NCU). (a) A longitudinal section through a dendritic shaft (d) bordered by several synaptic terminals. The end-foot (EF; pink-colored) between the neuropil and external capillary BL (oBL; blue) arbors its LC (arrow) as well as shafts of GCEs processes (purple and turquoise) and their parent boutons synapsing the dendrite. e = endothelium; pc = pericyte. (b) High-magnification view of the endfoot–endfoot intersection organizing a distinct gap junction between them. Arrowheads = glycogen particles. (c), (d), and (e) are progressive 3D views of the NCU. Two axo-dendritic synaptic terminals forming GCEs interacting with the LC of the oBL (outlined in blue). Dark green = dendritic shaft. (d) Three GCE-bearing terminals converging around the LC. (e) The neural elements as well as the BL are engulfed by the EF, which together with the underlying endothelium-PC furnishes the BPCU proper. (f) Diagram of the PUC in which the endothelial cell (gray) and PC processes (pale green) have been added. Note that GCEs accommodated next to the LC along the longitudinal axis, that is, parallel arrangement. Scale bars 0.5 μm in (a), 0.2 μm in (b). (g) Electron micrograph from the series reconstructed in "H" and "I." Oblique sections through the capillary wall showing two axo-spinous synapses (green) originate two GCEs -granule cell; in one of them (left) the terminal enlargement (arrow) lies next to the BL (purple). Note the endfoot (ef) surrounding the synaptic boutons. Arrowheads = external BL; light turquoise = dendritic spine. (h) and (i) are oblique and horizontal 3D views of the series encompassing three perivascular synaptic complexes with their respective GCE aligned along the longitudinal axis of the CBV. Scale bars = 0.5 μm in (A), 0.2 μm in (b), 1.0 μm in (c)–(e), and 0.5 μm in (g)–(i).

neuropil form long (i.e., >4 μm) pericapillary boutons. These boutons contain oval-to-flat synaptic vehicles that lack a discernable target (Figure 28d,e). Although EF also fully encases these terminals, no close apposition of them with the oBL could be identified.

## 3.6 | Blind nerve endings

Although no typical afferent terminals observed in peripheral receptors (Hashimoto, 1973; Rennels & Nelson, 1975) are observed in CBVs

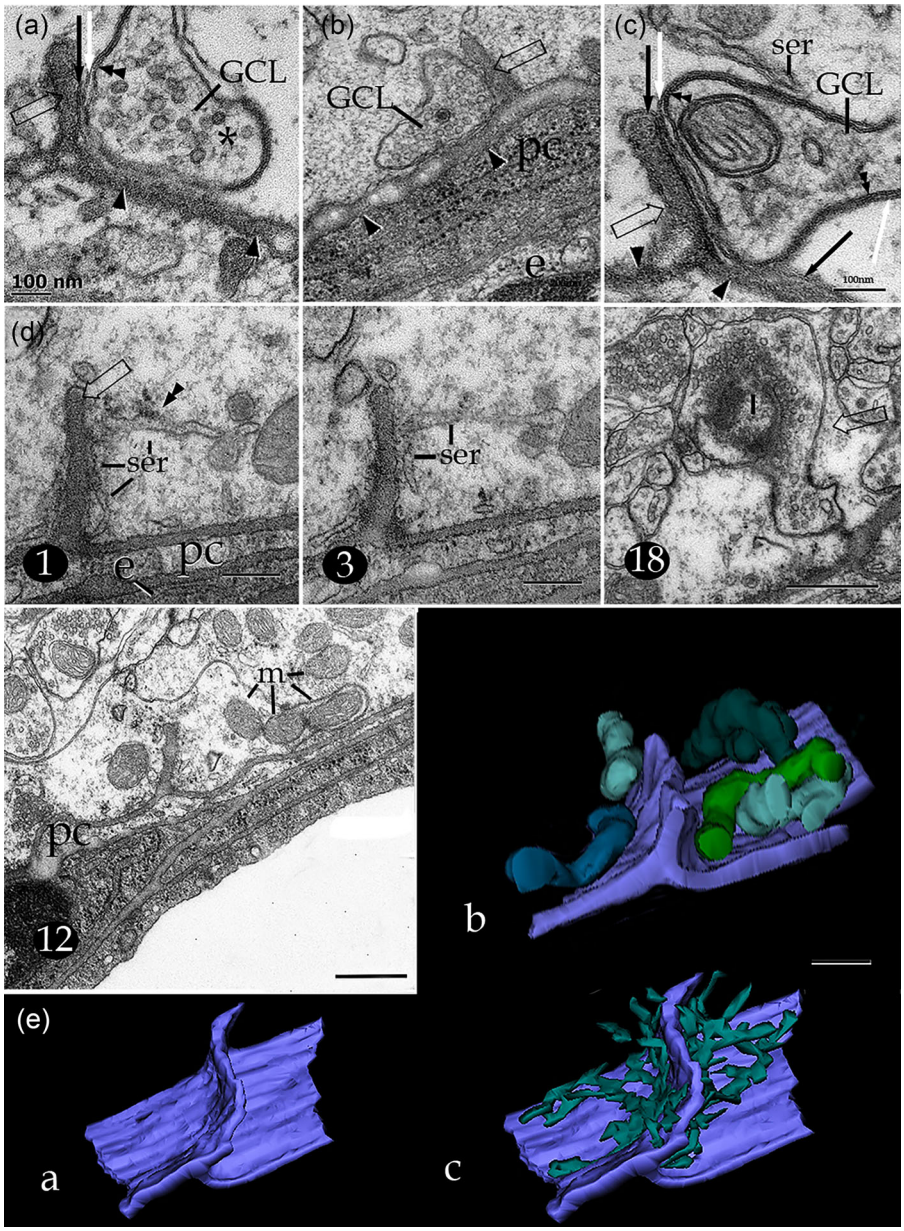


**FIGURE 17** Electron microscopic views of the GCE and the neighboring pericapillary region. (a) High-magnification micrograph encompassing the interaction of a GCE next to a LC (hollow arrow). Between them, there are 2-fold interposing inner (white arrow) and outer (black arrow) plasma membranes of the endfoot. Note the numerous small clear, rounded vesicles contained by the GCE cytoplasm (*). Double arrowhead = plasma membrane of the GCE; single arrowheads = outer capillary BL. (b) A GCE lying between the outer capillary BL (arrowheads) and an arising LC (hollow arrow). Note that the former structure contains numerous small rounded synaptic vesicles surrounding a solitary dense cored vesicle. pc = pericyte, e = endothelial cell. (c) High-magnification micrograph to depicting the astrocytic, double plasma membrane (arrows) dissecting the LC (hollow arrow), and the GCEe plasma membrane (double arrowhead); ser = smooth endoplasmic reticulum. (d) Assorted micrographs from a series encompassing 67 sections, the position in the series is designated by Arabic numerals at the lower left of the figure. Organelles of the end-foot cytoplasm (ef) associated with the LC (hollow arrows), consisting of smooth endoplasmic reticulum (ser) with scarce rough endoplasmic reticulum (double arrowheads). In Section 18, the enlarged, terminal portion of two GCEs (*) next to the LC is observed. m = mitochondria. (e) The LC and associated organelles are reconstructed from the series partially shown in "D." a = external BL and arising LC. b. mitochondria. c. Smooth endoplasmic reticulum. Scale bars = 100 nm (a)–(c), 0.2 μm in (d), 0.5 μm in Sections 12 and (e).

in the forebrain and brain stem specimens, two types of myelinated fibers can be observed in CBVs of the cerebellar cortex. The first type consists of myelinated axons approximating 0.8 to 1.5 μm in diameter. The axoplasm of these fibers loses myelin as it penetrates the CVB enveloped by the cuff formed by the EF. Therein, an axoplasmic outgrowth containing two or three distinct mitochondria courses toward the capillary oBL (Figure 29a,c). These terminals lack small synaptic vesicles, although few coated vesicles may be observed. The second type of myelinated axon that appears to terminate in the capillary wall is a thinner ending averaging 0.75 μm in diameter. Unlike the previ-

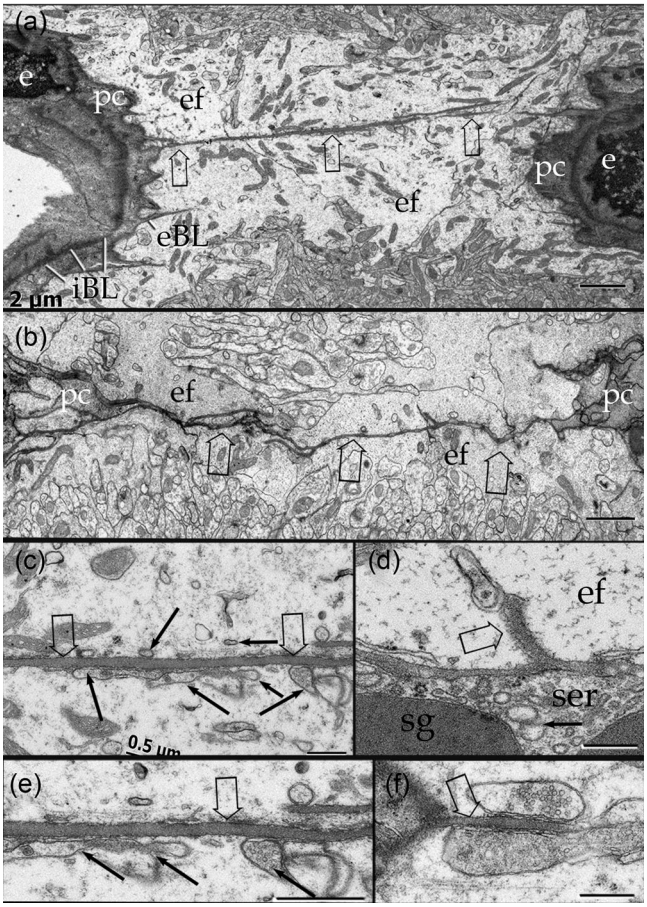


**FIGURE 18** Assorted electron micrographs depicting horizontal sections through LCs (hollow arrows). A. The section discloses an LC between two transversely sectioned CBVs with endothelial cells (e) and surrounding PC cytoplasm (pc) it can be observed on either side of the micrograph. Note the complete endfeet (ef) covering both oBL and LC proper. iBL = internal BL. (b) Another oBL LC (hollow arrows) bridging two CBVs with PC processes (pc) associated with the capillary wall on either side (not shown). (c) A segment of an oBL LC bounded by several terminal expansions (black arrows) of GCE. (d) Transverse section through an LC of the oBL overlapping the cytoplasm of a Mato cell with large secretory granules (sg) surrounded by numerous cisterns of the smooth endoplasmic reticulum (ser). (e) High-magnification view of optic field outlined in "C." Note the thin cytoplasmic layer (arrowheads) of the endfoot interposed between the LC and enlargements of the GCE. (f) An LC bounded by two terminal dilations of GCEs. Note the pleomorphic vesicles and the higher electron density of the GCE at the bottom of the figure, contrasting with the rounded vesicles of the upper GCE. Scale bars = 2 µm in (a) and (b); 0.5 µm in (c) to (f).

ous type, the axoplasm is virtually devoid of mitochondria; moreover, as soon as it approaches the capillary wall, it loses the myelin envelope. Like the axon itself, the terminal complex contains few microtubules, and its cell membrane is underscored by a fussy material containing scattered coated vesicles (Figure 29f(i)). Like the mitochondria-load terminal, the distal portion of this axon subtype is adjacent to the oBL and is always surrounded by an indistinct EF.

The findings of this study extend previous observations demonstrating novel structures in the perivascular neuropil in several brain regions of diverse mammalian species that we propose are involved in mechanosensory functions. To address the possible source of the specialized synaptic terminals that innervate the LCs, we analyzed the cerebellar cortex. The abovementioned description suggests that in this brain region, glutamatergic neurons are a source of projections to the perivascular neuropil structures characterized herein. Hence, we searched for vesicular glutamate terminals by immunostaining on the cerebellum of transgenic animals expressing the GFP reporter under the gene control of the astrocyte marker GFAP (Figure 30). Confocal image stacks allowed for the generation of 3D reconstructions that demonstrated the presence of glutamatergic terminals in close apposition to tunnels that we inferred as corresponding to CBVs and were enveloped by astrocytic cell extensions (Figure 30). Several of such terminals were located adjacent to nuclei that could correspond to pericytes and others seemed to be distant from these cells. Hence, these findings support the main notion of this work confirming the presence of what appears to be a TS in the perivascular region.

Moreover, according to our findings, perivascular mechanosensory structures are involved in detecting changes in blood pressure in the CBVs. Recent discoveries have shed light on the lingering question of the molecular mechanisms that transduce mechanical stimuli to neural signals (Nikolaev et al., 2015) as part of diverse afferent systems. The proteins piezo1 and piezo2, which are ion channels whereby their activity is modulated by mechanical influences, have been found to be key players in this issue. Therefore, we analyzed the expression of piezo1 in the rat brain telencephalon by using in situ hybridization. We observed the presence of piezo1 mRNA in the perinuclear region of cortical pyramidal (Figure 30b) and large thalamic neurons. Moreover, piezo1 mRNA expression was especially notable in pyramidal cells of the cortical parieto-temporal lobes and in the ventral tier of the thalamus. In the cerebellar cortex, we observed an expression signal in small clusters of piezo1 mRNA that matched cerebellar MF rosettes in location and dimensions (Figure 30c). Of these structures, some had punctate signals that could correspond to mRNA in the axon terminals, whereas others demonstrated signals consistent with the expression in endothelial cells themselves. Hence, these findings are consistent with the role of Piezo1 in the detection of mechanical signals in the brain and also demonstrated a higher complexity in the feedback system that regulates motor aspects of blood flow as commented upon in the next section.

## 4 | DISCUSSION

### 4.1 | Highlights of present observations

The fine structure and relevant features of the brain CBVs and surrounding neuropil are subsequently summarized. The first constraint relates to the general organization of the pericyte, which is known to be a fundamental cell type for genesis and blood flow regulation (Hirase et al., 2004) within blood vessels. Previously defined as the cell

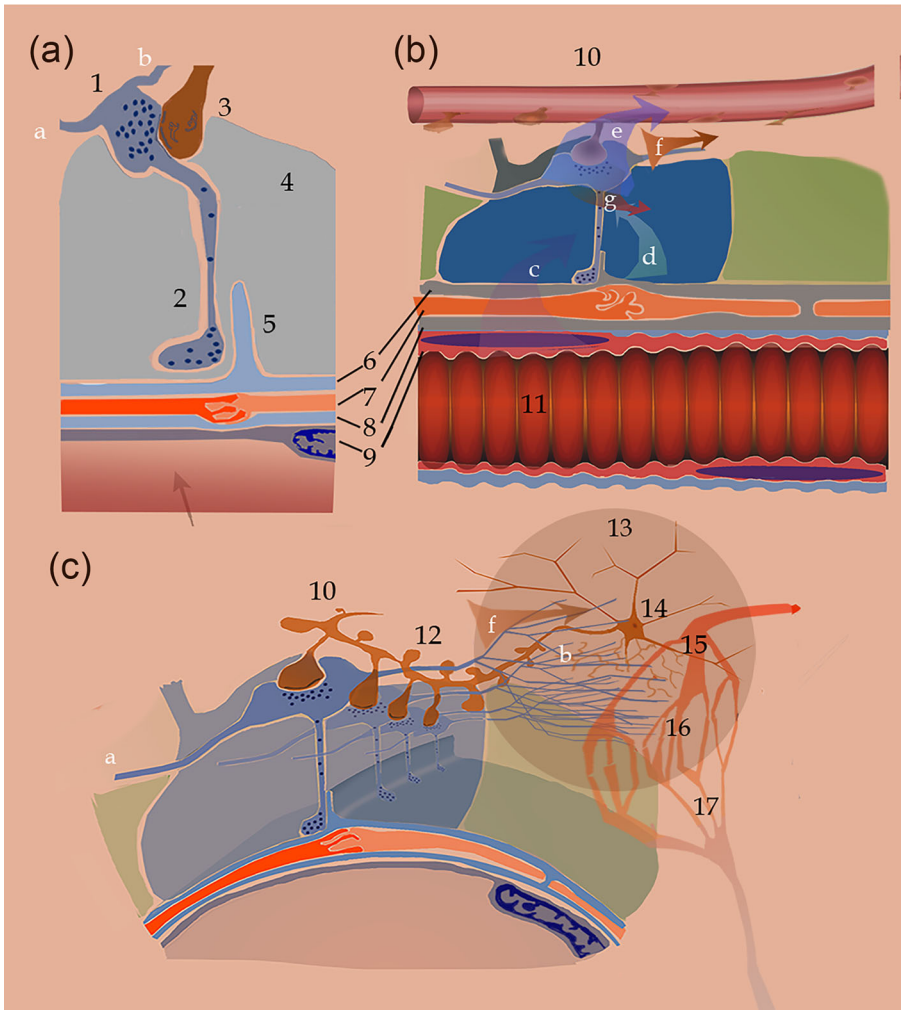


**FIGURE 19** Diagrammatic representation of the neocortex NCU. (a) Ascending thalamic-cortical nerve impulses originate axo (1)-spinous (3) synapses en passage (1 and 10), which extend GCE (2) ending next to an LC (5) and to the CBV proper. The endothelium (9) and interlacing PC(7) (orange) are surrounded by the inner (8) and outer BLs (6). The innermost endothelium (9) limits the capillary lumen (light orange-colored). Notice that the astrocytic endfoot (4) surrounds the synapse-GCE and prevents direct contact between the latter and the LC (5). a = proximal, b = distal axon. (b) Possible functional interactions of the capillary blood flow (11) with the NCU. The undulating profile of circulating red blood cells leads to an alternating displacement of the capillary wall. It is assumed that the frequency of such alternating displacement is directly related to the intensity of the blood flow (c). The low density of the EF cytoplasm (Lu et al., 2006; Walburg et al., 2006) facilitates propagation of pulsatile displacement (d), that eventually impacts the *Piezo1* expressing GCE-synapse controlling neurotransmitter release to the dendritic spine (e). Nerve impulses traveling in parent axon (a) proceed further (b). (c) Ascending nerve impulses travel in axons (a) to ramify (b) in the domain of the targeted neuronal circuit (13), where only one motoneuron is drawn (14). We propose that activation of 13, including 14, triggers vasodilation of arteriolar smooth muscle (15), intensity of blood flow in the capillary bed is monitored by the NCU (a) and recorded by efferent dendrite (12). If nerve impulses persist and the monitored blood flow satisfies the metabolic requirements of the neuronal domain (13), arteriolar muscle tone is kept constant. However, if blood flow within the capillary bed (16) or metabolic requirements in 13 are insufficient, motoneuron (14) induces further vasodilation. Conversely, increased blood flow or metabolite supply surpassing the needs of the neuronal domain 13 leads to a reduction of blood flow provoked by vasoconstriction. Thus, the vasomotor outcome results from the binomial effect of the frequency of nerve impulses arriving at the neuronal domain 13 and the blood flow intensity decoded by the NCU and transmitted to dendrites (12) of the motoneuron pool (14).

type that encircles the CBV itself (Zimmermann, 1923), in this study, a novel pericyte process, or string process bridging heteronymous CBVs of uneven diameter, was characterized. The discovery of a free pericyte lacking CBV and, subsequently, surrounded by neuropil and with a typical string process prompted the idea that it corresponds to a neuron; however, typical pericyte processes penetrate CBVs at either side. Additionally, pertaining to pericyte is another ubiquitous specialization that is known as the AP, and this process consists of a membranous structure that is frequently associated with sites of blood flow impact of the CBV (McDonald & Larue, 1983). The AP is first described and fully characterized in this study. A TS surrounded by EF was found to be specialized and crucial for neural interactions with the CBV. Thus, an earlier and masterful description of a functional neural–astroglial interaction (Araque et al., 1999) coupled with the observation that EF is a perivascular source of the third TS component (Cohen et al., 1996, 1997; Varela-Echevarría et al., 2017), suggests a physiological

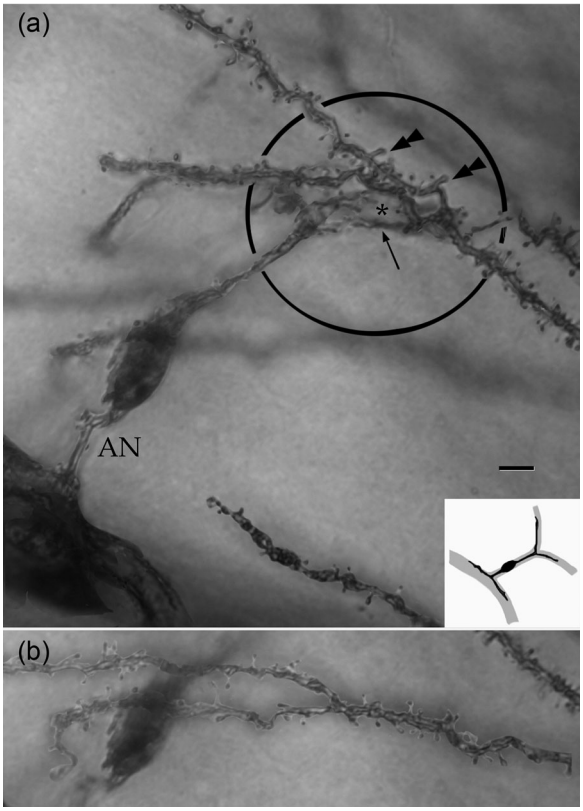


**FIGURE 20** Light microscopic digital photomontages of dendritic and axonal processes intersecting with the perivascular neuropil. (a) and (b) Distal pyramidal cell dendrites anchoring next to the secondary processes (circle) and perikaryon (pc) of a nearby PC (black-colored inset; d = dendrite). Notice that the overlaying dendrites originate in thicker spines (double arrowheads) and thin, supernumerary branchlets (arrows). Also, note the glial mantle (arrowhead) surrounding dendrites and distal PC processes. SP = string process with a discreet flexure. (b) Two perisomatic dendrites, one of them, encircles the cell body (arrow) of the PC shown in "A." (c) Neuropil associated with a longitudinally sectioned CBV (see inset). An axon collateral (arrowheads), issues short, transverse collaterals (*) that appear to terminate on two terminal dendrites (arrows). Scale bars = 3 μm.

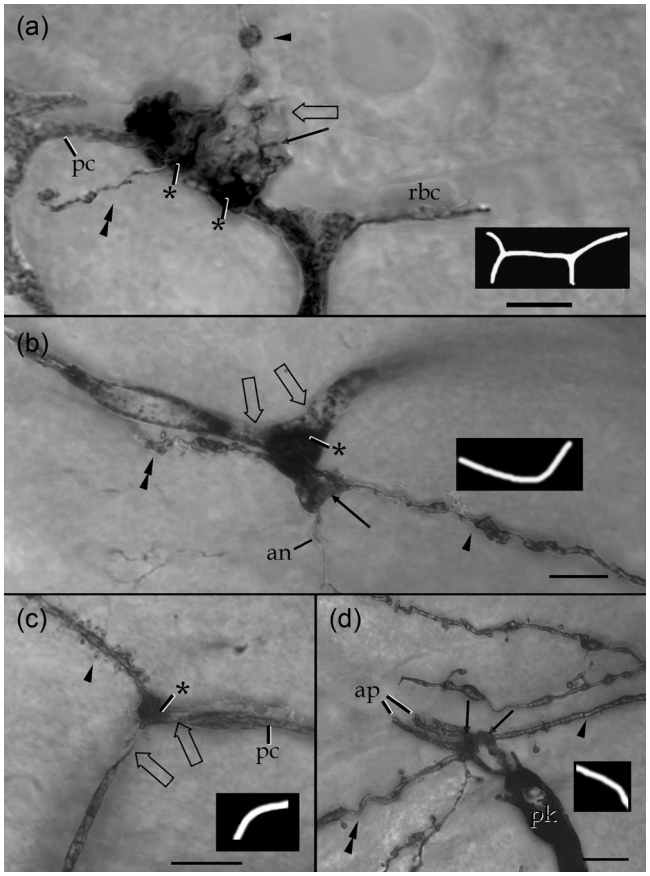


**FIGURE 21** Structural variations of dendritic processes within the pericapillary domain. The diagram at the lower left portion of the figure defines the capillary trajectory. (a) A terminal dendrite of an interneuron coursing from proximal (arrowhead) to distal (double arrowhead) within the pericapillary area assorted outgrowths (arrow) both of which appear masked by a glial envelope (hollow arrow). pc = pericyte processes; rbc = row of unstained red blood cells contained by the CBV. Parietal isocortex. (b) A solitary GC dendrite extending from proximal (arrowhead) to distal (double arrowhead). As the dendrite reaches the capillary wall it originates a large, rounded enlargement (*) engulfing the PC process (hollow arrows) surrounding the blood vessel. sp = perforating string process. (c) Terminal dendrite (arrowhead) of a medium-sized spiny cell that ends abruptly into a single, rounded enlargement (*) bounded by two PC processes (hollow arrows). Caudo-putamen nuclei. (d) Terminal dendrites of thalamic neurons, one of which overlaps the transverse limbs of the asymmetrical processes (ap). pk = perikaryon of a PC. Lateral thalamus. Scale bars = 3 μm.

relationship with the CBV proper. Due to the location and interaction between its paired branches, structural differentiation of the interstitial ground substance may play a mechanosensory role (Vega et al., 2009). Another previously unnoticed difference of pericapillary TSs is that synaptic terminals give rise to sets of tiny fibrils, which are referred to as GCEs. Series of GCEs link perivascular boutons with the oBL. More specifically, we observed a unique outgrowth that we termed LC. Strongly suggestive of a functional role is the strategic localization of the EF in association with the synapse-GCE and LC. Indeed, it is likely that the ability of peripheral astrocytic processes to control the availability of synaptic glutamate is shared by the EF. If so, $Ca^{++}$ oscillations influenced by blood flow may modulate the pericapillary synapse. Our 3D reconstructions demonstrated that GCEs arise from a series of perivascular synapses and are longitudinally aligned in the same order as parent boutons in the dendritic shaft (Figures 16 and 19). We suggest that the dendritic segment receiving a series of consecutive TSs and their GCE along the LC and underlying pericyte-endothelial cell furnish the NCU. These findings persuaded us to search for the cell type source of the unique pericapillary neuropil that was previously described in the initial part of this study. Due to the large number of short-axon and projecting neurons in the cerebral isocortex and thalamus, respectively, we opted for the cerebellar cortex, which has a relatively small number of known neurons (Palay & Chan-Palay, 1974; Ramón y Cajal, 1898). As in the forebrain NCU, cerebellar tributaries to the pericapillary domain were, invariably, encased by a dim

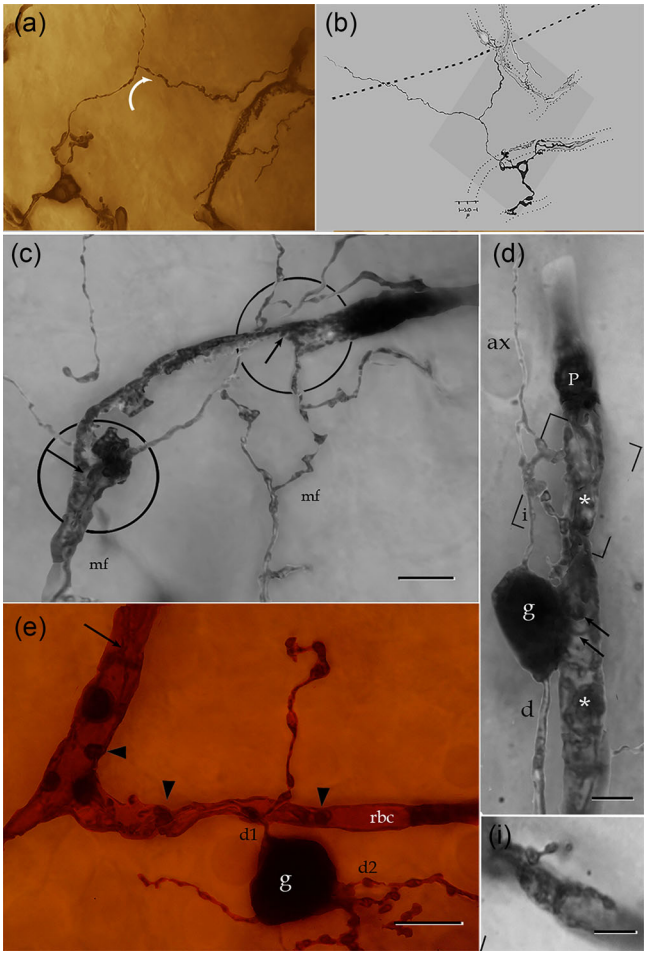


**FIGURE 22** Light microscopic views from the GC layer of the cerebellar cortex. (a) Photomontage from a GC with three divergent dendrites. In its ascending path, the axon sends a thicker collateral (arrow) that entangles with a CBV. (b) Camera lucida drawing of the neuron shown in "A." The lower magnification of the field shows the interaction of both the GC axon collateral (upper right) and dendrites entangling the capillary wall (dotted). A horizontal dotted line defines the boundaries between the GC and molecular layers. (c). Photomontage of the GC layer. Two ascending MF (mf) interact with PCs via a mossy fiber rossete (left) or short tongue-like excrescences (arrows) (see Figure 22d). (d) Photomontage of the intersection of the GC (g) perikaryon and its proximal processes with a PC surrounding the CBV. Notice the massive ramification of the axon collateral encircling (*) the underlying PC (p) as well as the short outgrowths of the perikaryon (arrows) (see Figure 21d). ax = distal axon, d = dendrite. (i) Single electron micrograph from the photomontage shown in "d". Notice the ramifying GC axon collateral encircling the external aspect of the capillary wall. (e) GCs originate from two divergent dendrites (d1 and d2), one of which (d1) ramifies next to the cell body into a horizontal branch with large beaded structureembedded in the capillary wall (arrowheads). Notice the distal processes (arrow) from a putative PC. rbc = red blood cell. Scale bars = 5 μm in (a), (b), (c), and (e), 2 μm in (d), 1 μm in (i). Adult rabbit, rapid-Golgi technique.

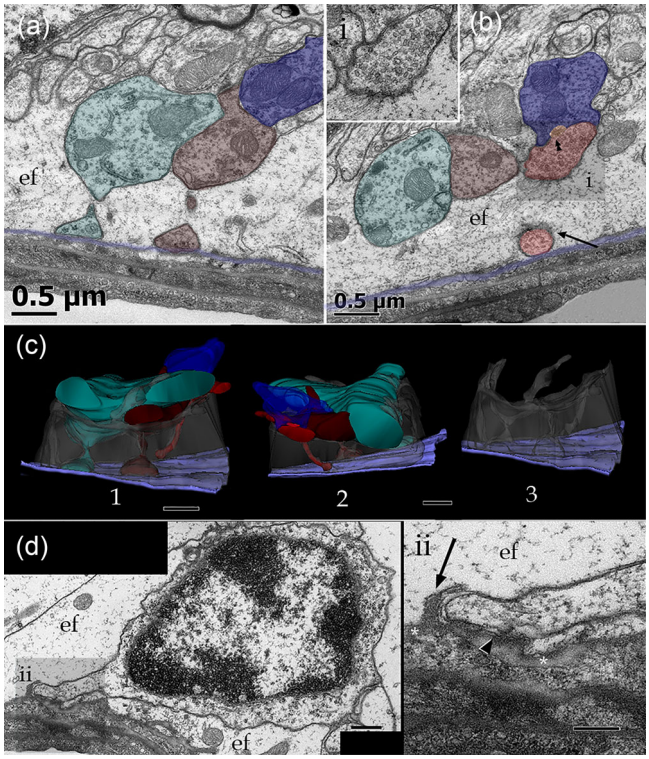


**FIGURE 23** Electron microscopic views of the granule cell (GC) layerof the cerebellar cortex. (a) Paired GC dendrites (green and pink-colored) originating homonymous spines lying next to the outer capillary BL (arrow). (b) Complementary micrograph from the same series as that of "A" in which an additional dendrite (blue) is contacted by a putative synaptic terminal from a stellate cell with a flat vesicle-containing bouton (red) gives rise to a GCE (arrow). Note that the latter structure anchors next to the outer capillary BL (light purple). Arrowheads = synaptic active zone. (i) = high-magnification view depicting the flat type of vesicles contained by the synaptic bouton. (c) Reconstructs from the complete series. 1 and 2. include dendrites (blue, green, and deep red). In 2, a Golgi cell axon with a synaptic terminal extends a GCE (bright red) structure contacting a dendritic shaft (blue) and descending next to the BL (light purple). Bright orange = active synaptic zone. 3. Image with the exclusion of the nerve processes visualizing the glial envelope provided by the end-foot (gray), precluding direct contact between the former structure and the BL. Orange = active synaptic zone. (d) Electron micrographs from a GC soma originating from a perivascular pseudopod anchoring next to the outer capillary BL. Note that the cell is completely engulfed by the endfeet (ef). (ii) High-magnification view disclosing the interaction of the GC pseudopod with the BL (*) and an arising LC (arrow), between them and the former structure, a thin cytoplasmic sheath (arrowhead) precludes direct contact. Calibration bars = 0.5 μm in (a) to (d), 0.2 μm in insets.

EF. The same scenario is applied to a small set of myelinated axons, which resembled sensory fibers (Banks, 1986). The possibility that a series of NCU along the capillary bed represents the afferent link to the motor vascular neuron pool compelled us to initially search first for

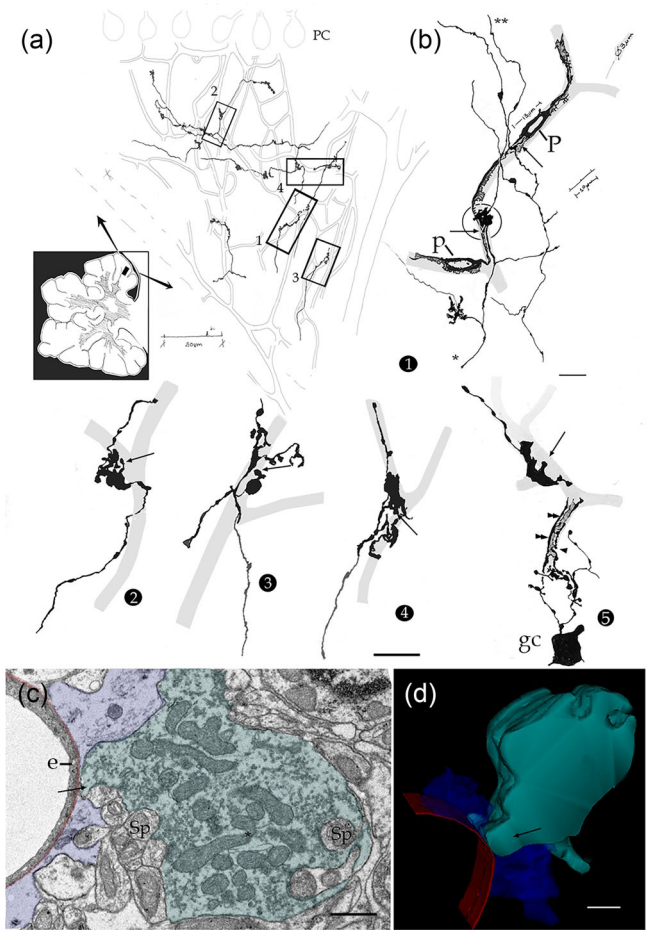


**FIGURE 24** Light and electron microscopic views of MFs in the cerebellar cortex. (a) Camera lucida drawings of blood vessels in the GC layer (soft pencil). MFs with synaptic boutons overlapping CBVs that have been drawn with black ink. (b) High-magnification drawings from MFs and synaptic boutons. Drawings designated 1 to 4 were obtained from the section shown in "A." 1. Two ascending MFs with those boutons that interact with PCs (p). Notice that the synaptic boutons extend short of passage outgrowths (arrows). CBVs are drawn with a soft pencil. * = proximal MF, ** = distal part of the MF. 2, 3, 4 and upper fiber in 5 are of passage outgrowths (arrow) from MF boutons. 5. A dendritic collateral from the granule cell (gc) lies in opposition to the secondary process (double arrowheads) of a PC (not shown). (c) A pericapillary MF terminal (green) protruding to the capillary BL (red), bounded by an endfoot (blue). e = endothelial cell, sp = GC dendritic spine. (d) 3D view from the MF terminal with distinct outgrowth (arrow) that penetrates between the endfoot (blue), next to the BL (red). Notice the indentations at the upper right of the bouton corresponding to GC dendritic spines. Calibration bars = 50 μm in (a), 10 in (b), 0.5 in (c) and (d).

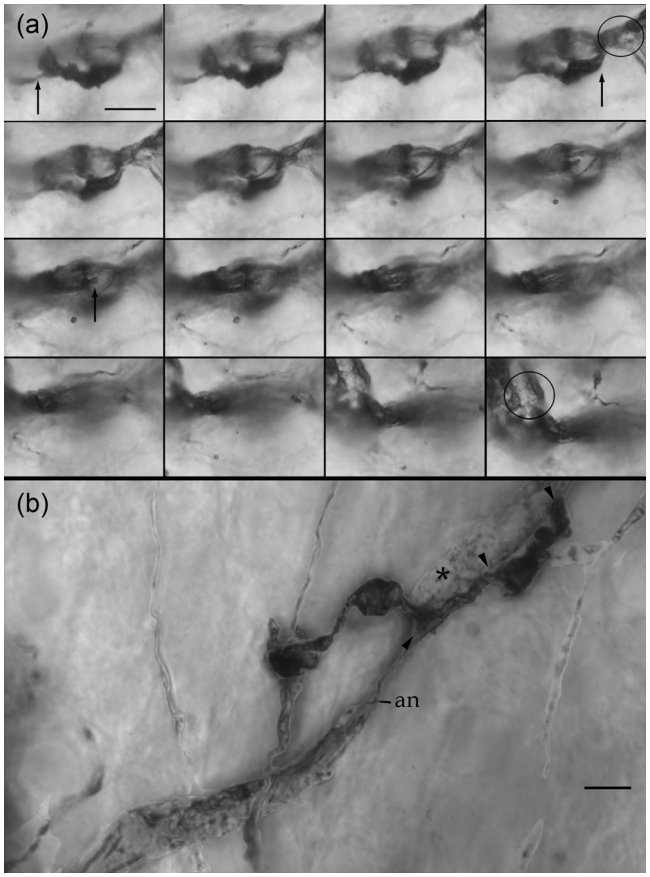


**FIGURE 25** Light microscopic photomontages of MFs. (a) Consecutive pictures at different focal depths illustrating the superposition of three synaptic outworths on the capillary wall. Notice the PC processes (circle) alternating with the synaptic outgrowths (arrows). (b) Singe MF alternating with three rosettes. Notice that the axonal shaft has three rosettes, with two of them extending short outgrowths overlapping the PC processes (&). sp = string process. Rapid-Golgi stain. Calibration bars = 2 μm.

the putative neurotransmitter that is associated with TS-GCEs. Synaptic boutons with clear, rounded vesicles establishing asymmetrical contacts with dendrites are the structural signature of glutamatergic synaptic transmission. Hence, immunoreactive sites to vesicular glutamate cotransporter 2 (vGLUT2) in the mouse cerebellum of the GFAP-GFP mouse with fluorescence in astrocytes (Nolte et al., 2001) were first identified. Importantly, we identified the expression of Piezo1 by in situ hybridization. Focal perivascular and pyramidal and putative projecting neurons expressing Piezo1 mRNA were observed in the cerebral cortex and thalamus, respectively. The finding that Piezo1 mRNA is contained by cerebellar MF rosettes, which represent a set of intimate CBV interactions supports the direct involvement of mechanoreception in modulating interneuron-projecting cell outcomes.

## 4.2 | Pericyte: Structure and interactions

First, observations of the CBV–pericyte interactions reveal novel structural peculiarities. From the early thorough description of the pericyte of euplacental mammals (Zimmerman, 1923), it has been known that this cell type organizes a flat, nearly continuous network encircling central and peripheral blood vessels. Although revising the vast current knowledge of the pericyte is beyond the scope of the present study, this cell type is fundamental in vascular genesis, metabolism, and

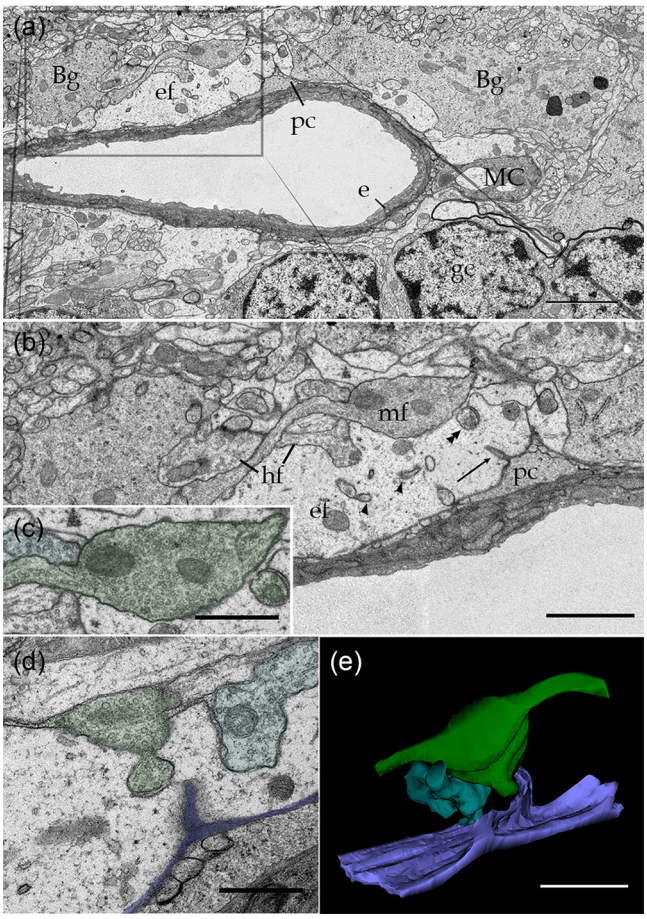


**FIGURE 26** Electron micrographs of the pericapillary neuropil at the superficial aspect of the cerebellar GC layer. (a) Tangential section through a CBV surrounded by Bergmann glial processes (Bg), Mato- (MC), granule-cells (gc), endfeet (ef) and nerve processes. (b) High-magnification view of the part of the area labeled in "A." Longitudinal section through a horizontal- (hf) and MF (mf) axons. The capillary wall is surrounded by the PC process (pc) underneath an LC (arrow), and electron-lucid endfeet (ef). The later structures are pierced by penetrating fibrils (arrowheads), possibly GCE. (c) High-magnification view of the mossy- (center) and horizontal (upper left) fibers. Note the tiny vesicle containing the appendage from the former. (d) Micrograph for another section of the series in which a frank protrusion is budding off from the MF terminal (green). An LC (blue) covering the PC process is observed. (e) 3D image from the series shown in (a) to (d). Note the synaptic outgrowth of the mossy- (green) and horizontal (turquoise) fiber terminals directed to the LC-BL (purple). Calibration bars 2 μm in (a), 0.5 μm in (b) to (e).

vasomotor activity. The contiguity of the pericyte with arterial smooth muscle fibers, which is another mural cell (Rouget, 1873), has led to the assumption that the pericyte subserves a vasomotor role (for reviews, see Iadecola & Nedergaard, 2007). However, direct in vivo observations of CBVs are consistent with the existence of subsets of annular mural cells expressing smooth muscle antigens alternating with longitudinal cells lacking such markers (Hill et al., 2015). This organization supports the idea that the pericyte provides a sensory network for the exchange of information between neural and vascular compartments (Hill et al., 2015). The interlacing processes of the pericyte, which is an electrically excitable cell (Hartmann et al., 2015) united by occasional gaps and numerous tight junctions, provide a potential physiological link between pericytes. Notably, interlacing pericyte processes protruding underneath the oBL-LC and united by gap and tight junctions suggest a joint functional interaction as well. However, until the precise physiological involvement of the pericyte-CBV is known, the functional implications of pericyte connectivity will remain an open question. Likewise, the tangential route defined by the perforating SP and the intercapillar pericyte was described in this study. The current SP appears to correspond to the solitary pericyte process identifiable in the illustrations by Zimmermann (1923). The SP leaves the parent pericyte-CBV and pierces the neighboring neuropil. The SP anchors on a second pericyte encircling a CBV of dissimilar diameter. Our observations provided new elements to the previous description of a perforating process in the human cerebral cortex (Shapson-Coe et al., 2021). Specifically, the novel identification of the SP as a distinct pericyte process, the asymmetry of CBVs linked by perforating SPs, and the pericyte with an outstanding location within the neuropil proper represent our innovative observations. The AP, which is another distinct membranous component, was also added to the cytological organization of the pericyte (Figures 2a and 10). Following its initial description with the Golgi technique, the electron microscopy provided several intrinsic and associated structures to the AP (Figure 12) all of which appear to be unified by a common functional (possibly sensory) role. This concept provides another putative sensory substratum to the long-standing dilemma of the reversible vasomotor activity elicited by functionally recruited areas of the brain, which is known as the blood-oxygen-level-dependent signal (BOLD) effect (Tsvetanov et al., 2020). The validity of these correlates remains open to future physiological assessments.

### 4.3 | Is the pericapillary endfoot a synergic sensory element?

The NCU is a highly specialized differentiation of the CBV-neuropil. It occurs in certain segments of the CBV characterized by thick EF covering, which is discernible with the light microscope (Figure 7b). Gaps present in the EF covering were commonly observed (Figure 5a–c), which contrasts with the complete EF covering of blood vessels of previous accounts (Mathiisen et al., 2010). At first observation, a high density of NCU in the isocortex and thalamus is evident by the distinct EF covering. Our results revealed fundamental evidence supporting the sensory involvement of the NCU in these brain regions, which represents the high incidence of associated TSs. Indeed, the starting point of the present study was our previous observation that sets of TSs in the cerebral isocortex and diencephalon are frequently engulfed by EF (Varela-Echevarría et al., 2017). The involvement of pericapillary EF synaptic interactions (Cohen et al., 1996, 1997) and of the EF itself responding to blood flow (Paulson & Neuman, 1987) and influencing both CBV diameter and the ensuing vasomotor response compelled our search for interactions between synapse-EF and the

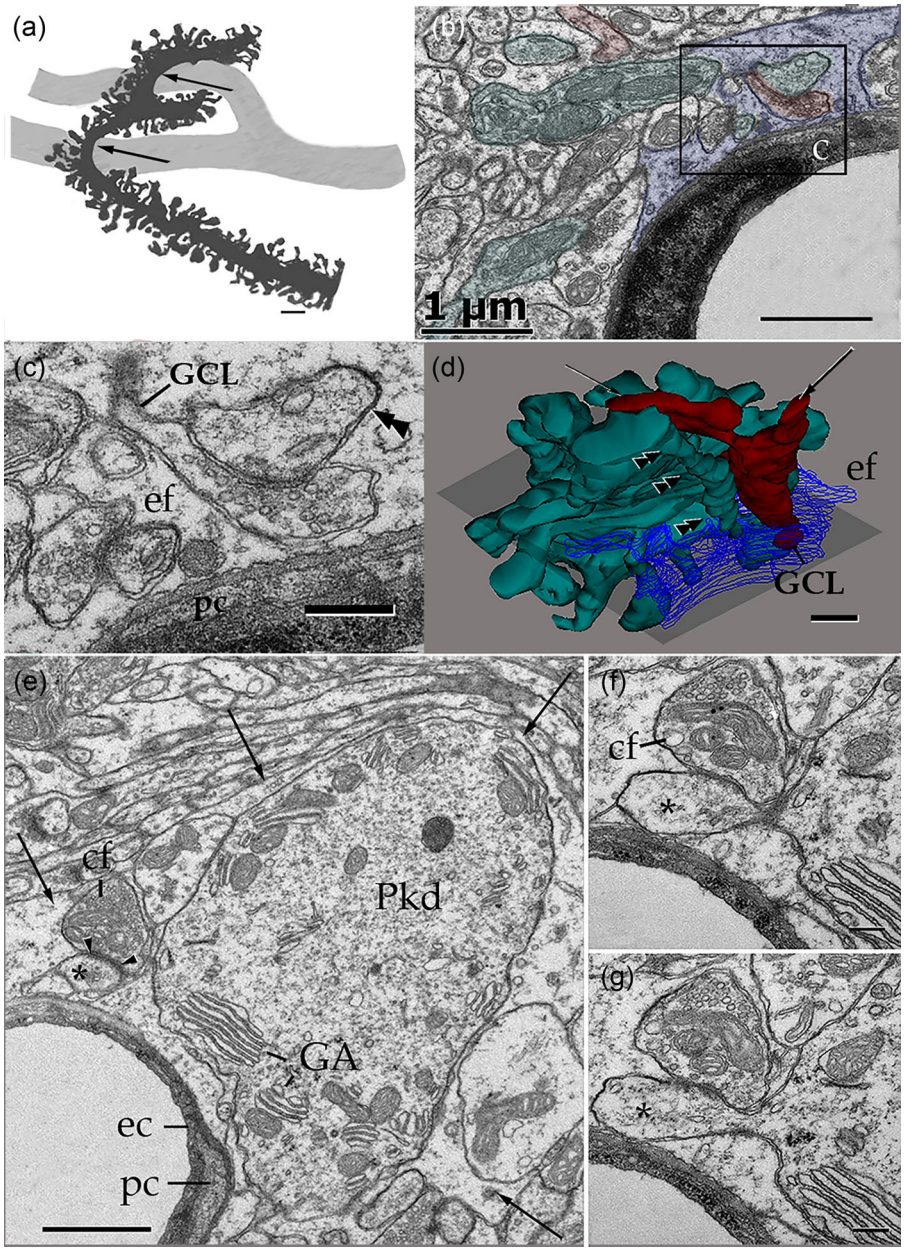


**FIGURE 27** Purkinje cell dendritic spines interact with parallel fiber terminals within the capillary wall. (a) High-magnification camera lucida drawing showing the impressions left (arrows) by two blood vessels (soft pencil), on a proximal dendrite of a Purkinje cell (black; PC). (b), (c), and (d), feature serial sections through a PC dendrite (green) Climbing fiber (red) gives rise to a GCE with a stem that had contacted the protruding dendritic spine (double arrowheads) stems of the climbing fiber (arrows). In (d), the endfoot (blue) has partially been reconstructed (ef) disclosing the full coverage to both dendritic and GCE processes. Note in (c) the numerous small rounded, clear vesicles contained by the synaptic bouton originating from the GCE. (e) to (g) are semiserial sections through a Purkinje dendritic process (PkD) extending a dendritic spine (*) encased by an end-foot (arrow) in what appears to be a TS. GA = Golgi apparatus. Calibration bars = 2 µm in (a); 1 µm in (b), (d), and (e); 0.2 µm in (c), (f), and (g).

CBV proper. Thus, the presence of numerous tiny tubular structures trapped by the EF cytoplasm (Figure 18c–f) prompted the use of serial sections. Surprisingly, we found that the enigmatic fibrils piercing the EF correspond to extensions of the synaptic bouton organizing the TS. Moreover, the ubiquity of the new ultrastructural anatomical feature of precapillary central synapses (now termed GCEs) along with their alignment to the LC and to the opposing alpha and beta AP linked by tiny fibrils in the ground substance (Schwartz & DeSimone, 2008; Vega et al., 2009) suggest that they correspond to mechanical-transducing structures. Notably, GCEs necessitate transducing elements to yield mechanical energy EF membrane $Ca^{++}$ oscillations (Burdyga & Borysova, 2018; Deitmer et al., 2009; Neuman et al., 1984; Paulson & Neuman, 1987; Windship et al., 2007) or receptor potentials (RPs) and neuron retrieval (Anenberg et al., 2015; Shmuel et al., 2002, 2006; Tsvetanov, 2020; Vaucher et al., 2000). An important clue regarding this effect was provided by the vesicle content of both

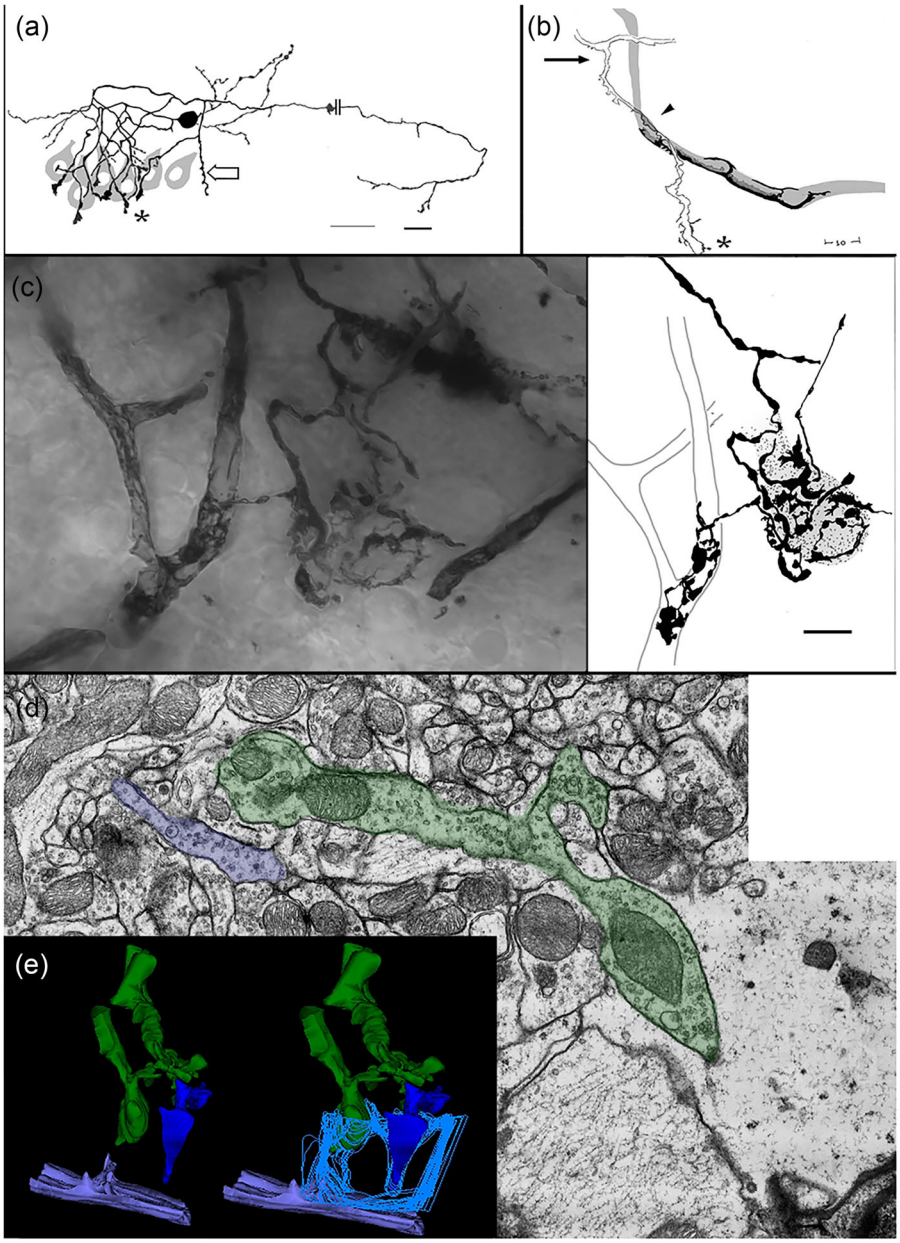


**FIGURE 28** Light and electron microscopic views of cerebellar basket cell and its perivascular axon processes. (a) Survey camera lucida drawing of a basket cell in that part of the molecular layer intersecting with Purkinje cell somata (gray). The long axon of the former structure gives rise to thick, vertical extensions, or pinceau that insinuate the latter. Thinner, varicose fibrils (hollow arrows) are the second axonal specialization. (b) High-magnification drawing of the root of a thick collateral (arrow) that helicoidally surround a nearby CBV (soft pencil) encased by PC processes (black). * = pinceau. (c) High-magnification views of a pericellular basket surrounding an unstained Purkinje cell perikaryon. Sidewise, the basket extends a varicose-type axon that, correspondingly, entangles the capillary wall, thus masking the PC processes (arrow). The full axons are drawn on the right side of the figure, outlying the capillary contour and the Purkinje cell soma (soft pencil) (d). Electron micrograph from a series illustrating parts of two presumptive distal axons (colored) of a basket cell. Axon endings (one not shown) (green) contain oval and occasional flat synaptic vesicles and a single mitochondrion (e). 3D reconstructions of the full 93 sections. The left side reconstruction includes the two fibrils with their respective boutons (green and blue) and the capillary outer BL with a protruding LC. The endfoot (light blue) enveloping both terminals is outlined at the right side reconstruction. Calibration bars in (a) to (c) = 10 μm, 0.5 μm in (d), (e).

perivascular synaptic bouton-GCE typical of glutamatergic, excitatory synapses (Clascá et al., 2012; Palay & Chan-Palay, 1974; Uchizono, 1975). Indeed, the EF surrounding a series of axo-dendritic boutons giving rise to an ordered set of GCEs next to the oBL-LC strongly suggests a sensory role. A plausible interpretation of these anatomical findings is that mechanical stimuli could modify the EF $Ca^{++}$ oscillations, thus modulating synaptic transmission (Schipke & Kettenmamm, 2004) and impacting the GCE-synaptic output to its dendritic tribu-

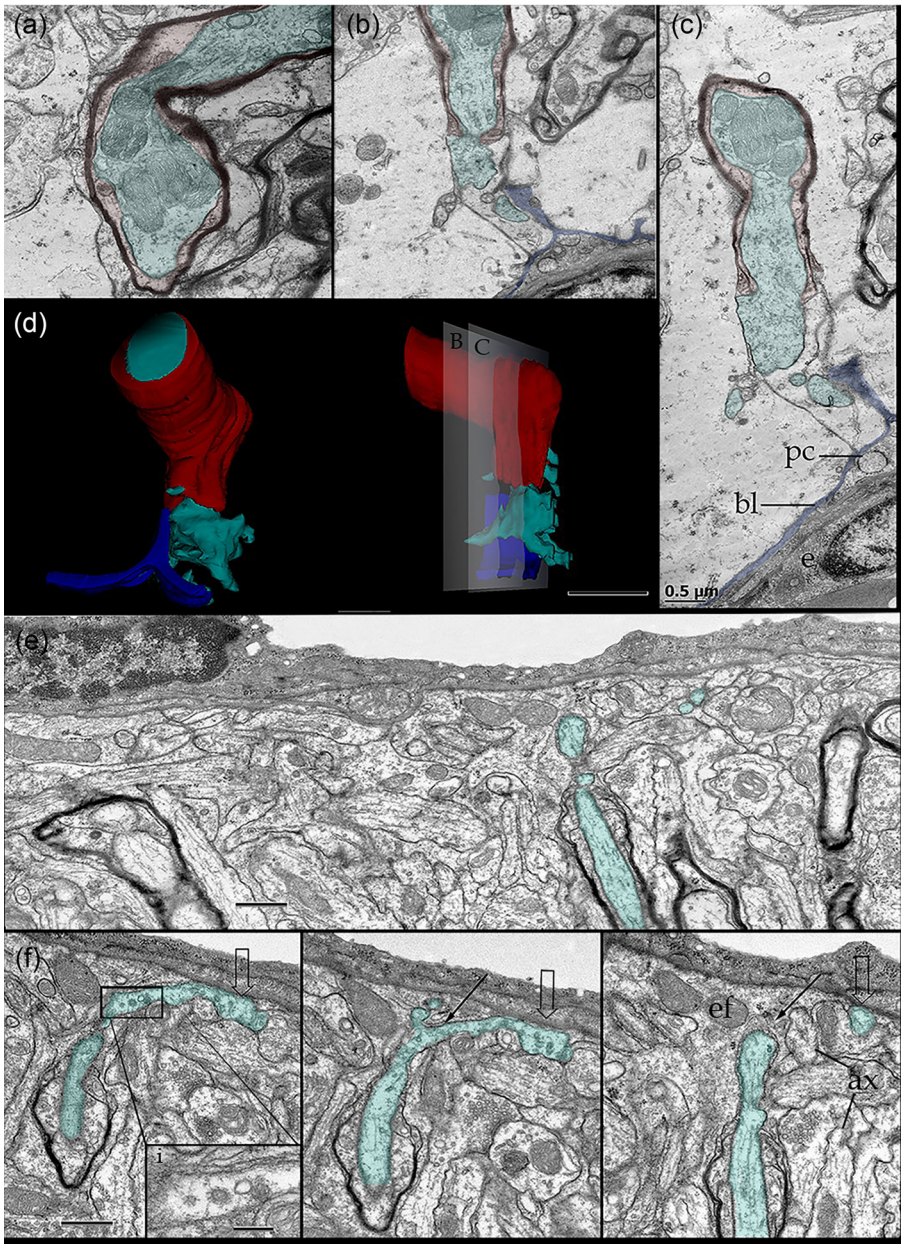


**FIGURE 29** Series encompassing putative afferent or blind nerves in the cerebellar cortex. (a), (b), and (c) Alternating micrographs through a myelinated nerve extending a bizarre outgrowth that is entirely engulfed by an endfoot (ef). Notice that prior to losing the myelin envelope the axoplasm is filled by a cluster of mitochondria (m) that are, otherwise, absent in the nude axoplasm (&). bl = BL; e = endothelium; pc = PC processes. (d) Reconstructions of the terminal axon that had lost the myelin envelope (red) expands (green) in the perivascular area adjacent to an LC arising from the outer BL (blue). (e) Three terminal axons as assessed in a series encompassing them. A nude, narrow axoplasmic outgrowth (green) approaching the capillary wall of one of the capillaries (green). (f) Subsequent series of that section is shown in "E" defining the full distal axon trajectory to resolve (hollow arrow) next to the outer BL surrounded by an endfoot (ef). (i) High-magnification of the axoplasm containing coated vesicles. Notice the axoplasmic outgrowth of another nearby blind axon. (ax). Calibration bars: 1.0 µm.

tary or to the parent axon (Figure 19). Although the definition of the chemical nature of the synaptic GCE (Sy-GCE) is still in progress, the vesicle content coupled with our immunohistochemical observations supports both the cell of origin and its glutamatergic nature. The putative sequence of capillary mechanical events to neuron retrieval and vasomotor response is summarized in Figure 19.

## 4.4 | Thalamic and cortical neurons are the source of pericapillary synaptic terminals

The possible existence of baroreceptor ion channels within the perivascular domain is highly relevant to our current hypothesis of the mechanosensory role of the NCU. Thus, we analyzed the expression of

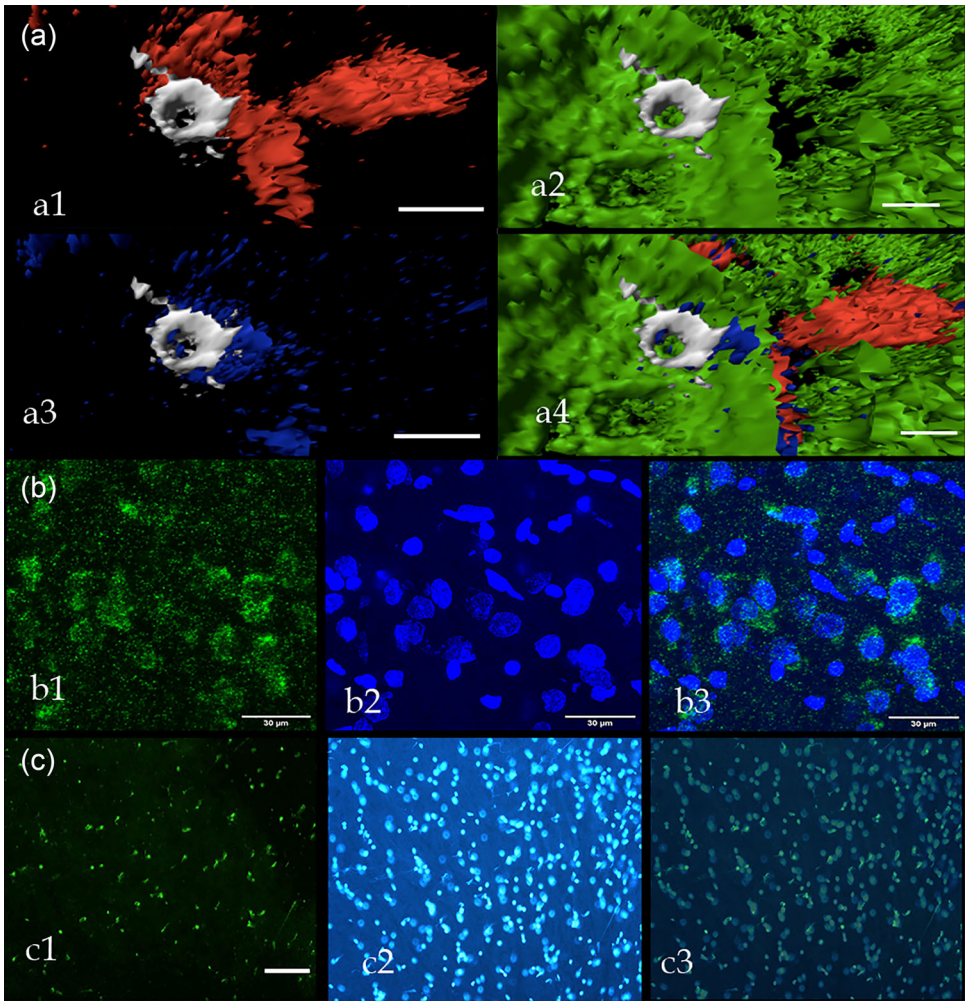


**FIGURE 30** In situ hybridization and confocal, immunohistochemistry. (a) Triple immunocytochemistry for CGRP (red) B4 isolectin (IB4) (white), vGlut2 (blue) and eGRP (green). a1 endothelium (white) CGRP, a2 eGRP and IB4, a3. IB4, a3. vGlut2 and IB4, a4 croop. (b) In situ hybridization of *Piezo1* mRNA in layer V of the parietal lobe. b1 mRNA-*Piezo1*, b2 nuclei, b3 crop. (c) In situ hybridization of Piezo1 mRNA in the cerebellum deep GC layer. c1 Piezo1 mRNA probe. c2 nuclei. c3 croop. Calibration bars in (a) = 10 μm, 20 μm in (b) and (c), (i = 0.2 μm.

the Piezo1 mechanosensitive channel gene by using in situ hybridization. Our light microscopic evidence of Piezo1 mRNA throughout the capillary wall (data not shown) is also observable in large glutamatergic synaptic complexes such as the MF (Figure 30c). This indirect evidence, coupled with the ubiquitous distribution of *Piezo 1* and *Piezo 2* in the vascular endothelium (J. Li et al., 2014) in peripheral blood vessels and in the pericapillary domain, supports the possibility that together with TS-GCE-LC, the brain CBV endothelium is also responsible for the process of mechanical transduction. Our results favor the viewpoint that mechanical transduction may occur within the synapse-GCE, which is supported by the significant Piezo1 expression in both pyramidal and thalamic neurons, which represent the main source of cortical glutamatergic synapses. Therefore, as pyramidal and thalamic neurons express Piezo1 mRNA (Figure 30b) and are the chief source of the asymmetrical Sy-GCEs, it is reasonable that mechanical disturbances impacting the CVB wall are transmitted by the EF low viscosity (Lu et al., 2006) eliciting $Ca^{++}$ signaling, which recruits (Bezzi et al., 2004) the aligned Sy-GCEs and, ultimately, influences the dendritic processes of the neuron motor pool (Figure 19; Hill et al., 2015; Shmuel, 2002, 2006,). Currently, the possibility that the stem axon originating Sy-GCE is retrogradely recruited must be left as an open question. Aside from the present postulate requiring further immunocytological and physiological assessments, another basic dilemma arises regarding the neuronal identity of axons and dendritic tributaries to dendrite-Sy-GCE (Figure 19).

## 4.5 | Pericapillary synapses set dual, reciprocal interactions

Although the previous information pertains to the putative sensory role of the NCU, a possible afferent–efferent (i.e., dual) role should also be considered as it is commonly observed in most peripheral sensory organs (Banks, 1986, 2015; Bewick & Banks, 2015). Indeed, the early identification of synaptic vesicles in primary afferent axons constituted a puzzling observation (Kruger, 1988). However, electron microscopic

studies with vesicle tracing techniques have demonstrated that a set of synaptic vesicles in sensory nerve terminals correspond to recycling elements. Furthermore, subsequent cytochemical research provided direct evidence for vGlut2 release enhancing receptor output (Bewick & Banks, 2015; Zhang et al., 2018). The omnipresence of coated vesicles associated with positivity to vGut2 supports their involvement in a possible tuning role of the receptor potential. However, more recent observations (Bopp et al., 2017) in the sensory and motor cortex have indicated that synaptic structures with or without coated vesicles may coexist with vGlut2 immunoreactivity (Fujiyama et al., 2001). The possible presence of vGlut2 ir associated with the NCU would lend strong support to a reciprocal functional link between the GCE-synaptic bouton and the EF-capillary wall (see Banks, 2015). Therefore, we performed combined immunohistochemistry for vGlut2 and CGRP, landmark molecules for sensory receptor axon identification (Iijima & Zhang, 2002; Silverman & Kruger, 1990; Zhang et al., 2018) and blood flow modulation (Brain & Grant, 2004). Our results demonstrate regions in which vGlut2 and GCRP are present in sites corresponding to the NCU. Hence, the presumptive mechanotransduction ascribed to the NCU may be subject to vGlut2-mediated reciprocal modulation at the CGRP ir (Zhang et al., 2018) delivered by ascending and afferent tracts, which, in our opinion, constitute the source of GCE synapses. Although the presence of synaptic terminals in dendrites within the CBV-neuropil intersection may seem trivial, we believe that it is highly significant for two reasons. First, it can serve as a possible mechanism to decode temporal and spatial inputs from aligned synapses representing longitudinal GCE-LCs successions along the CBV (Figures 16 and 19). Second, their parent neurons are defined. Our observations in the forebrain demonstrated that dendrites of principal neurons intersect with CBVs. To address the question on neuronal identity, we selected the cerebellar cortex because its main afferences and neuron types (Ramón y Cajal, 1904) as well as the surrounding neuropil have been thoroughly studied (Hamory & Somogyi, 1983; Palay & Chan-Palay, 1974; Sotelo, 2008), thus providing us with a foundation to interpret electron microscopic observations.

## 4.6 | MF as a sensory element

Our first approach via the Golgi technique demonstrated a unique set of axonal and dendritic tributaries to cortical cerebellar CBVs. In fact, we believe that the CBV contribution should be added to Cajalt's basic circuitry. For instance, in comparing the direct Cajal axonal path traced by the GC to the molecular layer, we discovered a unique collateralization of the GC axon to the CBV (Figure 22a,b) and identified a distinct somatic and dendritic contribution to CBVs (Figures 22e and 23). Although the wealth of information provided by the Golgi technique could not always be correlated with our electron microscopic observations, a necessary first step to understanding the organization of the cerebellar perivascular neuropil is provided. Two ascending fiber systems defined by the mossy (Figures 22c and 24) and parallel fibers (Figure 22a,b) display obvious, chiefly passage contributions to the pericapillary neuropil. Furthermore, GCs, MFs, and ascending parallel fibers modulated by Golgi neurons represent the chief source of glutamatergic terminals to the interneuron-Purkinje cell chain. Therefore, the possibility arises that brain stem volleys of nerve impulses arriving at the cerebellar cortex are reciprocally modulated by the EF–CBV interaction; thus, the red blood cell column impacts (Moore & Cao, 2008; Noguchi & Gommper, 2005) influence the eventual synaptic targets of ascending axons.

We addressed this scenario by searching for Piezo1 mechanosensitive channels, whose ganglion cell expression is necessary to elicit the peripheric homeostatic baroreflex (Zeng et al., 2018). The present demonstration of Piezo2 mRNA expression in pyramidal isocortical cells and deep cerebellar nuclei (Wang & Hamil, 2021) opens the possibility of central mechanosensory decoding. Furthermore, the existence of endothelial mechano-sensitive Piezo1 channels in peripheral blood vessels (J. Li et al., 2014) and Piezo2 in the ganglion cell-mechanoreceptor unit (Woo et al., 2015), coupled with the frequent CBV-MF rosette interaction, led us to further investigate a possible Piezo1 baroreceptor channel associated with them. Hence, we cloned the Piezo1 gene and provided molecular evidence (in situ hybridization) for the expression of this gene in ventral thalamus pyramidal cells of the isocortex, and in large, scattered foci matching the cerebellar MF rosette in both size and distribution (Figure 30c). Overall, the interaction of CBV organizing TS with Piezo1 mRNA expressing MF rosettes linked with granule and Golgi cells (Mapelli & D'Angelo, 2007) may modulate the eventual vasomotor response (G. Yang & Idecola, 1996) that is performed by stellate and Purkinje cells outputs. This putative functional interaction provides a molecular and cellular foundation to account for the episodic vasomotor response provoked by cortical cerebellar neuronal recruitment.

## 4.7 | CONCLUSION REMARKS

Altogether, our observations indicate that the forebrain's NCU is a complex interplay of the forebrain vasculature that has a dual role in the modulation of blood flow in relation to local neuronal activity. The arteriolar muscular tone is rapidly inhibited secondary to neuronal excitation and restored upon return to baseline neuronal activity. The resulting bimodal recruitment of afferent axons, corticalcircuits, and arteriolar smooth muscle, results in a fast, reversible increment of capillary blood flow that underpins the BOLD signal.

The existence of cytological and molecular substrates transducing endogenous mechanical stimuli delivered by blood flow is highly relevant to numerous processes within the nervous system. Thus, the putative hemodynamic-sensing structures described in this study provide an essential mechanistic element in the decoding of blood flow resulting in an effective vasomotor response. Experimental testing of this postulate in future studies is feasible with electrophysiological, molecular, pharmacological, and behavioral strategies.

### ACKNOWLEDGMENTS

The 3D image processing was performed at the Laboratorio Nacional de Visualización Científica Avanzada (LAVIS) with the support of Ale-

jandro de León Cuevas, Alejandro Ávalos Fernández, and Luis A. Aguilar Bautista. Technical support was also provided by Adriana González Gallardo, Michael Jeziorsky Ma. Antonieta Carbajo, Loudes Palma, Martín García Servín. The last version of our manuscript was proofed by American Journal Experts.

## CONFLICT OF INTEREST STATEMENT

I, Jorge Antonio Larriva-Sahd, on behalf of doctors: Gema Martínez-Cabrera, Carlos Lozano-Flores, Luis Concha, and Alfredo Varela-Echavarría, co-authors of the manuscript entitled: "The neurovascular unit of CBVs in the rat nervous system. A rapid-Golgi electron microscopic study," intended for publication in the *Journal of Comparative Neurology*, express that our work has not a conflict of interest in terms of patent and ownership, and none of us is member of a company board directors, an advisory board, or committee for a company, neither consultancy for or receipt of speaker's fees from a company.

## DATA AVAILABILITY STATEMENT

The data that support the findings of this study are available from the corresponding author upon reasonable request.

## ORCID

*Jorge Larriva-Sahd* https://orcid.org/0000-0002-7254-0773

## REFERENCES

Anenberg, E., Chan, A. W., Xie, Y., LeDue, J. M., & Murphy, T. H. (2015). Optogenetic stimulation of GABA neurons can decrease local neuronal activity while increasing cortical blood flow. *Journal of Cerebral Blood Flow & Metabolism*, *35*(10), 1579–1586. https://doi.org/10.1038/jcbfm.2015.140

Araque, A., Parpura, V., Sanzgiri, R. P., & Haydon, P. G. (1999). Tripartite synapses: Glia, the unacknowledged partner. *Trends in Neurosciences*, *22*(5), 208–215. https://doi.org/10.1016/s0166-2236(98)01349-6

Armulik, A., Genové, G., Mäe, M., Nisancioglu, M. H., Wallgard, E., Niaudet, C., He, L., Norlin, J., Lindblom, P., Strittmatter, K., Johansson, B. R., & Betsholtz, C. (2010). Pericytes regulate the blood–brain barrier. *Nature*, *468*(7323), 557–561. https://doi.org/10.1038/nature09522

Bandettini, P. A., Wong, E. C., Hinks, R. S., Tikofsky, R. S., & Hyde, J. S. (1992). Time course EPI of human brain function during task activation. *Magnetic Resonance in Medicine*, *25*(2), 390–397. https://doi.org/10.1002/mrm.1910250220

Banks, R. W. (1986). Observations on the primary sensory ending of tenuissimus muscle spindles in the cat. *Cell and Tissue Research*, *246*(2), 309–319. https://doi.org/10.1007/bf00215893

Banks, R. W. (2015). The innervation of the muscle spindle: A personal history. *Journal of Anatomy*, *227*(2), 115–135. https://doi.org/10.1111/joa.12297

Berthiaume, A.-A., Hartmann, D. A., Majesky, M. W., Bhat, N. R., & Shih, A. Y. (2018). Pericyte structural remodeling in cerebrovascular health and homeostasis. *Frontiers in Aging Neuroscience*, *10*, 210. https://doi.org/10.3389/fnagi.2018.00210

Bertossi, M., Virgintino, D., Maiorano, E., Occhiogrosso, M., & Roncali, L. (1997). Ultrastructural and morphometric investigation of human brain capillaries in normal and peritumoral tissues. *Ultrastructural Pathology*, *21*(1), 41–49. https://doi.org/10.3109/01913129709023246

Bewick, G. S., & Banks, R. W. (2015). Mechanotransduction in the muscle spindle. *Pflügers Archiv—European Journal of Physiology*, *467*(1), 175–190. https://doi.org/10.1007/s00424-014-1536-9

Bezzi, P., Gundersen, V., Galbete, J. L., Seifert, G., Steinhäuser, C., Pilati, E., & Volterra, A. (2004). Astrocytes contain a vesicular compartment that is competent for regulated exocytosis of glutamate. *Nature Neuroscience*, *7*(6), 613–620. https://doi.org/10.1038/nn1246

Bopp, R., Holler-Rickauer, S., Martin, K. A. C., & Schuhknecht, G. F. P. (2017). An ultrastructural study of the thalamic input to layer 4 of primary motor and primary somatosensory cortex in the mouse. *The Journal of Neuroscience*, *37*(9), 2435–2448. https://doi.org/10.1523/jneurosci.2557-16.2017

Boulay, A.-C., Saubaméa, B., Adam, N., Chasseigneaux, S., Mazaré, N., Gilbert, A., Bahin, M., Bastianelli, L., Blugeon, C., Perrin, S., Pouch, J., Ducos, B., Le Crom, S., Genovesio, A., Chrétien, F., Declèves, X., Laplanche, J.-L., & Cohen-Salmon, M. (2017). Translation in astrocyte distal processes sets molecular heterogeneity at the gliovascular interface. *Cell Discovery*, *3*(1), 17005. https://doi.org/10.1038/celldisc.2017.5

Brain, S. D., & Grant, A. D. (2004). Vascular actions of calcitonin gene-related peptide and adrenomedullin. *Physiological Reviews*, *84*(3), 903–934. https://doi.org/10.1152/physrev.00037.2003

Bruns, R. R., & Palade, G. E. (1968). Studies on blood capillaries: I. General organization of blood capillaries in muscle. *Journal of Cell Biology*, *37*(2), 244–276. https://doi.org/10.1083/jcb.37.2.244

Burdyga, T., & Borysova, L. (2018). $Ca^{2+}$ signalling in pericytes. In A. Birbrair (Ed.), *Pericyte biology—Novel concepts: Advances in experimental medicine and biology* (Vol. 1109, pp. 95–109). Springer Nature.

Cauli, B., & Hamel, E. (2010). Revisiting the role of neurons in neurovascular coupling. *Frontiers in Neuroenergetics*, *2*, 9. https://doi.org/10.3389/fnene.2010.00009

Chaigneau, E., Oheim, M., Audinat, E., & Charpak, S. (2003). Two-photon imaging of capillary blood flow in olfactory bulb glomeruli. *Proceedings of the National Academy of Sciences of the United States of America*, *100*(22), 13081–13086. https://doi.org/10.1073/pnas.2133652100

Chan-Palay, V., & Palay, S. L. (1970). Interrelations of basket cell axons and climbing fibers in the cerebellar cortex of the rat. *Zeitschrift für Anatomie und Entwicklungsgeschichte*, *132*(3), 191–227. https://doi.org/10.1007/bf00523377

Chan-Palay, V., & Palay, S. L. (1971). The synapse en marron between Golgi II neurons and mossy fibers in the rat's cerebellar cortex. *Zeitschrift für Anatomie und Entwicklungsgeschichte*, *133*(3), 274–287. https://doi.org/10.1007/bf00519303

Clascá, F., Rubio-Garrido, P., & Jabaudon, D. (2012). Unveiling the diversity of thalamocortical neuron subtypes. *European Journal of Neuroscience*, *35*(10), 1524–1532. https://doi.org/10.1111/j.1460-9568.2012.08033.x

Cohen, Z., Molinatti, G., & Hamel, E. (1997). Astroglial and vascular interactions of noradrenaline terminals in the rat cerebral cortex. *Journal of Cerebral Blood Flow & Metabolism*, *17*(8), 894–904. https://doi.org/10.1097/00004647-199708000-00008

Cohen, Z. V. I., Bonvento, G., Lacombe, P., & Hamel, E. (1996). Serotonin in the regulation of brain microcirculation. *Progress in Neurobiology*, *50*(4), 335–362. https://doi.org/10.1016/s0301-0082(96)00033-0

Deitmer, J. W., Singaravelu, K., & Lohr, C. (2009). Calcium ion signaling in astrocytes. In P. Haydon & V. Parpura (Eds.), *Astrocytes in (patho)physiology of the nervous system* (pp. 201–224). Springer.

Dimitriadou, V., Aubineau, P., Taxi, J., & Seylaz, J. (1987). Ultrastructural evidence for a functional unit between nerve fibers and type II cerebral mast cells in the cerebral vascular wall. *Neuroscience*, *22*(2), 621–630. https://doi.org/10.1016/0306-4522(87)90358-7

Dubový, P., & Bednárová, J. (1999). The extracellular matrix of rat Pacinian corpuscles: An analysis of its fine structure. *Anatomy and Embryology*, *200*(6), 615–623. https://doi.org/10.1007/s004290050309

Fujiwara, T., & Uehara, Y. (1984). The cytoarchitecture of the wall and the innervation pattern of the microvessels in the rat mammary gland: A scanning electron microscopic observation. *American Journal of Anatomy*, *170*(1), 39–54. https://doi.org/10.1002/aja.1001700104

Fujiyama, F., Furuta, T., & Kaneko, T. (2001). Immunocytochemical localization of candidates for vesicular glutamate transporters in the rat cerebral cortex. *The Journal of Comparative Neurology*, *435*(3), 379–387. https://doi.org/10.1002/cne.1037

Graeber, M. B., & Streit, W. J. (1990). Perivascular microglia defined. *Trends in Neurosciences*, *13*(9), 366. https://doi.org/10.1016/0166-2236(90)90020-b

Grinvald, A., Frostig, R. D., Siegel, R. M., & Bartfeld, E. (1991). High-resolution optical imaging of functional brain architecture in the awake monkey. *Proceedings of the National Academy of Sciences of the United States of America*, *88*(24), 11559–11563. https://doi.org/10.1073/pnas.88.24.11559

Hama, K., Arii, T., & Kosaka, T. (1994). Three-dimensional organization of neuronal and glial processes: High voltage electron microscopy. *Microscopy Research and Technique*, *29*(5), 357–367. https://doi.org/10.1002/jemt.1070290506

Hámori, J., & Somogyi, J. (1983). Differentiation of cerebellar mossy fiber synapses in the rat: A quantitative electron microscope study. *The Journal of Comparative Neurology*, *220*(4), 365–377. https://doi.org/10.1002/cne.902200402

Hartmann, D. A., Underly, R. G., Grant, R. I., Watson, A. N., Lindner, V., & Shih, A. Y. (2015). Pericyte structure and distribution in the cerebral cortex revealed by high-resolution imaging of transgenic mice. *Neurophotonics*, *2*(4), 041402. https://doi.org/10.1117/1.nph.2.4.041402

Hashimoto, K. (1973). Fine structure of the Meissner corpuscle of human palmar skin. *Journal of Investigative Dermatology*, *60*(1), 20–28. https://doi.org/10.1111/1523-1747.ep13069657

Hawkins, B. T., & Davis, T. P. (2008). The blood-brain barrier/neurovascular unit in health and disease. *Pharmacological Reviews*, *57*(2), 173–185. https://doi.org/10.1124/pr.57.2.4

Hernandez-Linares, Y., Olvera, A., Villalobos, P., Lozano-Flores, C., Varela-Echavarria, A., Luna, M., & Orozco, A. (2019). 3,5-T2 and 3,3',5-T3 regulate cerebellar thyroid hormone signalling and myelin molecular dynamics in Tilapia. *Scientific Reports*, *9*(1), 7359. https://doi.org/10.1038/s41598-019-43701-w

Hill, R. A., Tong, L., Yuan, P., Murikinati, S., Gupta, S., & Grutzendler, J. (2015). Regional blood flow in the normal and ischemic brain is controlled by arteriolar smooth muscle cell contractility and not by capillary pericytes. *Neuron*, *87*(1), 95–110. https://doi.org/10.1016/j.neuron.2015.06.001

Hirase, H., Creso, J., Singleton, M., Barthó, P., & Buzsáki, G. (2004). Two-photon imaging of brain pericytes in vivo using dextran-conjugated dyes. *Glia*, *46*(1), 95–100. https://doi.org/10.1002/glia.10295

Iadecola, C. (2004). Neurovascular regulation in the normal brain and in Alzheimer's disease. *Nature Reviews Neuroscience*, *5*(5), 347–360. https://doi.org/10.1038/nrn1387

Iadecola, C. (2017). The neurovascular unit coming of age: A journey through neurovascular coupling in health and disease. *Neuron*, *96*(1), 17–42. https://doi.org/10.1016/j.neuron.2017.07.030

Iadecola, C., & Nedergaard, M. (2007). Glial regulation of the cerebral microvasculature. *Nature Neuroscience*, *10*(11), 1369–1376. https://doi.org/10.1038/nn2003

Iijima, T., & Zhang, J.-Q. (2002). Three-dimensional wall structure and the innervation of dental pulp blood vessels. *Microscopy Research and Technique*, *56*(1), 32–41. https://doi.org/10.1002/jemt.10007

Jakab, R. L., & Hámori, J. (1988). Quantitative morphology and synaptology of cerebellar glomeruli in the rat. *Anatomy and Embryology*, *179*(1), 81–88. https://doi.org/10.1007/bf00305102

Jones, E. G. (1970). On the mode of entry of blood vessels into the cerebral cortex. *Journal of Anatomy*, *106*, 507–520.

Jung, S.-H., Kim, S., Chung, A.-Y., Kim, H.-T., So, J.-H., Ryu, J., Park, H.-C., & Kim, C.-H. (2009). Visualization of myelination in GFP-transgenic zebrafish. *Developmental Dynamics*, *239*(2), 592–597.

Kruger, L. (1988). Chapter 28 Morphological features of thin sensory afferent fibers: A new interpretation of 'nociceptor' function. In W. Hamman & A. Iggo (Eds.), *Progress in brain research* (pp. 253–257). Elsevier.

Larriva-Sahd, J. (2006). Histological and cytological study of the bed nuclei of the stria terminalis in adult rat. II. Oval nucleus: Extrinsic inputs, cell types, neuropil, and neuronal modules. *The Journal of Comparative Neurology*, *497*(5), 772–807. https://doi.org/10.1002/cne.21011

Larriva-Sahd, J. (2008). The accessory olfactory bulb in the adult rat: A cytological study of its cell types, neuropil, neuronal modules, and interactions with the main olfactory system. *The Journal of Comparative Neurology*, *510*(3), 309–350. https://doi.org/10.1002/cne.21790

Larriva-Sahd, J., León-Olea, M., Vargas-Barroso, V., & Varela-Echavarría, A. (2019). On the existence of mechanoreceptors within the neurovascular unit of the rodent and rabbit brain. *Brain Structure and Function*, *224*, 2247–2267. https://doi.org/10.1007/s00429-019-01863-3

Lee, K. J., Kim, H., & Rhyu, I. J. (2005). The roles of dendritic spine shapes in Purkinje cells. *The Cerebellum*, *4*(2), 97–104. https://doi.org/10.1080/14734220510007842

Li, J., Hou, B., Tumova, S., Muraki, K., Bruns, A., Ludlow, M. J., Sedo, A., Hyman, A. J., McKeown, L., Young, R. S., Yuldasheva, N. Y., Majeed, Y., Wilson, L. A., Rode, B., Bailey, M. A., Kim, H. R., Fu, Z., Carter, D. A., Bilton, J., … Beech, D. J. (2014). Piezo1 integration of vascular architecture with physiological force. *Nature*, *515*(7526), 279–282. https://doi.org/10.1038/nature13701

Li, N., Zhang, X., Dong, H., Hu, Y., & Qian, Y. (2017). Bidirectional relationship of mast cells-neurovascular unit communication in neuroinflammation and its involvement in POCD. *Behavioural Brain Research*, *322*, 60–69. https://doi.org/10.1016/j.bbr.2017.01.006

Lu, Y.-B., Franze, K., Seifert, G., Steinhäuser, C., Kirchhoff, F., Wolburg, H., Guck, J., Janmey, P., Wei, E.-Q., Käs, J., & Reichenbach, A. (2006). Viscoelastic properties of individual glial cells and neurons in the CNS. *Proceedings of the National Academy of Sciences of the United States of America*, *103*(47), 17759–17764. https://doi.org/10.1073/pnas.0606150103

Mapelli, J., & D'Angelo, E. (2007). The spatial organization of long-term synaptic plasticity at the input stage of cerebellum. *The Journal of Neuroscience*, *27*(6), 1285–1296. https://doi.org/10.1523/jneurosci.4873-06.2007

Mathiisen, T. M., Lehre, K. P., Danbolt, N. C., & Ottersen, O. P. (2010). The perivascular astroglial sheath provides a complete covering of the brain microvessels: An electron microscopic 3D reconstruction. *Glia*, *58*(9), 1094–1103. https://doi.org/10.1002/glia.20990

Mato, M., Ookawara, S., & Kurihara, K. (1980). Uptake of exogenous substances and marked infoldings of the fluorescent granular pericyte in cerebral fine vessels. *American Journal of Anatomy*, *157*(3), 329–332. https://doi.org/10.1002/aja.1001570308

Mato, M., Ookawara, S., Sakamoto, A., Aikawa, E., Ogawa, T., Mitsuhashi, U., Masuzawa, T., Suzuki, H., Honda, M., Yazaki, Y., Watanabe, E., Luoma, J., Yla-Herttuala, S., Fraser, I., Gordon, S., & Kodama, T. (1996). Involvement of specific macrophage-lineage cells surrounding arterioles in barrier and scavenger function in brain cortex. *Proceedings of the National Academy of Sciences of the United States of America*, *93*(8), 3269–3274. https://doi.org/10.1073/pnas.93.8.3269

Mato, M., Ookawara, S., Sugamata, M., & Aikawa, E. (1984). Evidence for the possible function of the fluorescent granular perithelial cells in brain as scavengers of high-molecular-weight waste products. *Experientia*, *40*(4), 399–402. https://doi.org/10.1007/bf01952574

Mazanet, R., & Franzini-Armstrong, C. (1982). Scanning electron microscopy of pericytes in rat red muscle. *Microvascular Research*, *23*(3), 361–369. https://doi.org/10.1016/s0026-2862(82)80008-3

McCaslin, A. F. H., Chen, B. R., Radosevich, A. J., Cauli, B., & Hillman, E. M. C. (2011). In vivo 3D morphology of astrocyte-vasculature interactions in the somatosensory cortex: Implications for neurovascular coupling. *Journal of Cerebral Blood Flow & Metabolism*, *31*(3), 795–806. https://doi.org/10.1038/jcbfm.2010.204

McDonald, D. M., & Larue, D. T. (1983). The ultrastructure and connections of blood vessels supplying the rat carotid body and carotid sinus. *Journal of Neurocytology*, *12*(1), 117–153. https://doi.org/10.1007/bf01148090

Moore, C. I., & Cao, R. (2008). The hemo-neural hypothesis: On the role of blood flow in information processing. *Journal of Neurophysiology*, *99*(5), 2035–2047. https://doi.org/10.1152/jn.01366.2006

Munger, B., Yoshida, Y., Hayashi, S., Osawa, T., & Idé, C. (1988). A reevaluation of the cytology of cat Pacinian corpuscles. I. The inner core and clefts. *Cell and Tissue Research*, *253*(1), 83–93. https://doi.org/10.1007/BF00221743

Newman, E. A., Frambach, D. A., & Odette, L. L. (1984). Control of extracellular potassium levels by retinal glial cell K + siphoning. *Science*, *225*(4667), 1174–1175. https://doi.org/10.1126/science.6474173

Nikolaev, Y. A., Dosen, P. J., Laver, D. R., van Helden, D. F., & Hamill, O. P. (2015). Single mechanically-gated cation channel currents can trigger action potentials in neocortical and hippocampal pyramidal neurons. *Brain Research*, *1608*, 1–13. https://doi.org/10.1016/j.brainres.2015.02.051

Noguchi, H., & Gompper, G. (2005). Shape transitions of fluid vesicles and red blood cells in capillary flows. *Proceedings of the National Academy of Sciences of the United States of America*, *102*(40), 14159–14164. https://doi.org/10.1073/pnas.0504243102

Nolte, C., Matyash, M., Pivneva, T., Schipke, C. G., Ohlemeyer, C., Hanisch, U.-K., Kirchhoff, F., & Kettenmann, H. (2001). GFAP promoter-controlled EGFP-expressing transgenic mice: A tool to visualize astrocytes and astrogliosis in living brain tissue. *Glia*, *33*(1), 72–86. https://doi.org/10.1002/1098-1136(20010101)33:1⟨72::aid-glia1007⟩3.0.co;2-a

Ogawa, S., Tank, D. W., Menon, R., Ellermann, J. M., Kim, S. G., Merkle, H., & Ugurbil, K. (1992). Intrinsic signal changes accompanying sensory stimulation: Functional brain mapping with magnetic resonance imaging. *Proceedings of the National Academy of Sciences of the United States of America*, *89*(13), 5951–5955. https://doi.org/10.1073/pnas.89.13.5951

Palay, S. L., & Chan-Palay, V. (1974). *Cerebellar cortex: Cytology and organization*. Springer.

Paulson, O. B., & Newman, E. A. (1987). Does the release of potassium from astrocyte endfeet regulate cerebral blood flow? *Science*, *237*(4817), 896–898. https://doi.org/10.1126/science.3616619

Peters, A., Palay, S. L., & Webster, F. (1976). *The Fine Structure of the Nervous System: The Neurons and Supporting Cells*. Philadelphia: W.B. Saunders Company.

Ramón y Cajal, S. (1904). *Textura del Sistema Nervioso Central del Hombre y Los Vertebrados*. (L. Moya, Ed.), Madrid.

Rechenbach, A., & Herting, W. (2009). Structural association of astrocytes with neurons and vasculature: Defining territorial boundaries. In Astrocytes V. Parpura, & P. G. Haydon (Eds.), *Astrocytes in (Patho) Physiology of the Nervous System* (p. 251). Springer Science. https://doi.org/10.1007/978-0-387-79492-1_10

Reichenbach, A., & Wolburg, H. (2005). Astrocytes and ependymal glia. In H. Kettenmann, & B. Ransom (Eds.), *Neuroglia* (pp. 19–35). New York: Oxford University Press.

Rennels, M. L., & Nelson, E. (1975). Capillary innervation in the mammalian central nervous system: An electron microscopic demonstration. *American Journal of Anatomy*, *144*(2), 233–241. https://doi.org/10.1002/aja.1001440208

Ribatti, D. (2015). The crucial role of mast cells in blood–brain barrier alterations. *Experimental Cell Research*, *338*(1), 119–125. https://doi.org/10.1016/j.yexcr.2015.05.013

Rouget, D. (1873). Mémoire sur le développement la structure et les propriétés. Physiologiques des capillaires sanguins et lymphatiques. *Arch Physiol Norm Path*, *5*, 603–663.

Roy, C. S., & Sherrington, C. S. (1890). On the regulation of the blood-supply of the brain. *The Journal of Physiology*, *11*(1-2), 85–158. https://doi.org/10.1113/jphysiol.1890.sp000321

Schipke, C. G., & Kettenmann, H. (2004). Astrocyte responses to neuronal activity. *Glia*, *47*(3), 226–232. https://doi.org/10.1002/glia.20029

Schwartz, M. A., & DeSimone, D. W. (2008). Cell adhesion receptors in mechanotransduction. *Current Opinion in Cell Biology*, *20*(5), 551–556. https://doi.org/10.1016/j.ceb.2008.05.005

Shapson-Coe, A., Januszewski, M., Berger, D. R., Pope, A., Wu, Y., Blakely, T., Schalek, R. L., Li, P. H., Wang, S., Maitin-Shepard, J., Karlupia, N., Dorkenwald, S., Sjostedt, E., Leavitt, L., Lee, D., Bailey, L., Fitzmaurice, A., Kar, R., Field, B., … Lichtman, J. W. (2021). *A connectomic study of a petascale fragment of human cerebral cortex*. https://doi.org/10.1101/2021.05.29.446289

Shmuel, A., Augath, M., Oeltermann, A., & Logothetis, N. K. (2006). Negative functional MRI response correlates with decreases in neuronal activity in monkey visual area V1. *Nature Neuroscience*, *9*(4), 569–577. https://doi.org/10.1038/nn1675

Shmuel, A., Yacoub, E., Pfeuffer, J., Van de Moortele, P.-F., Adriany, G., Hu, X., & Ugurbil, K. (2002). Sustained negative BOLD, blood flow and oxygen consumption response and its coupling to the positive response in the human brain. *Neuron*, *36*(6), 1195–1210. https://doi.org/10.1016/s0896-6273(02)01061-9

Silverman, J. D., & Kruger, L. (1990). Selective neuronal glycoconjugate expression in sensory and autonomic ganglia: Relation of lectin reactivity to peptide and enzyme markers. *Journal of Neurocytology*, *19*, 789–801.

Sims, D. E. (1986). The pericyte—A review. *Tissue and Cell*, *18*(2), 153–174. https://doi.org/10.1016/0040-8166(86)90026-1

Somogyi, P., & Smith, A. D. (1979). Projection of neostriatal spiny neurons to the substantia nigra. Application of a combined golgi-staining and horse-radish peroxidase transport procedure at both light and electron microscopic levels. *Brain Research*, *178*(1), 3–15. https://doi.org/10.1016/0006-8993(79)90084-2

Sotelo, C. (2008). Viewing the cerebellum through the eyes of Ramón y Cajal. *The Cerebellum*, *7*(4), 517–522. https://doi.org/10.1007/s12311-008-0078-0

Starborg, T., Lu, Y., Kadler, K. E., & Holmes, D. F. (2008). Electron microscopy of collagen fibril structure in vitro and in vivo including three-dimensional reconstruction. *Extracellular Matrix and Cell Junctions*, *89*, 319–345. https://doi.org/10.1016/S0091-679X(08)00417-2

Swanson, L. W. (2004). *Brain maps III: Structure of the rat brain*. Elsevier.

Tsvetanov, K. A., Henson, R. N. A., & Rowe, J. B. (2020). Separating vascular and neuronal effects of age on fMRI BOLD signals. *Philosophical Transactions of the Royal Society B: Biological Sciences*, *376*(1815), 20190631. https://doi.org/10.1098/rstb.2019.0631

Uchizono, K. (1975). *Excitation and inhibition. Synaptic morphology*. Igaku Shoin Ltd.

Ushiwata, I., & Ushiki, T. (1990). Cytoarchitecture of the smooth muscles and pericytes of rat cerebral blood vessels. *Journal of Neurosurgery*, *73*(1), 82–90. https://doi.org/10.3171/jns.1990.73.1.0082

Varela-Echevarría, A., Vargas-Barroso, V., Lozano-Flores, C., & Larriva-Sahd, J. (2017). Is there evidence for myelin modeling by astrocytes in the normal adult brain? *Frontiers in Neuroanatomy*, *11*, 75. https://doi.org/10.3389/fnana.2017.00075

Vaucher, E., Tong, X.-K., Cholet, N., Lantin, S., & Hamel, E. (2000). GABA neurons provide a rich input to microvessels but not nitric oxide neurons in the rat cerebral cortex: A means for direct regulation of local cerebral blood flow. *The Journal of Comparative Neurology*, *421*(2), 161–171. https://doi.org/10.1002/(sici)1096-9861(20000529)421:2⟨161::aid-cne3⟩3.0.co;2-f

Vega, J. A., García-Suárez, O., Montaño, J. A., Pardo, B., & Cobo, J. M. (2009). The Meissner and Pacinian sensory corpuscles revisited new data from the last decade. *Microscopy Research and Technique*, *72*(4), 299–309. https://doi.org/10.1002/jemt.20651

Walburg, H., Guck, J., Janmey, P., Wei, E. Q., Kas, J., & Reichenbach, A. (2006). Viscoelastic properties of individual glial cells and neurons in the CNS. *Proceedings of the National Academy of Sciences of the United States of America*, *103*, 17759–17764. https://doi.org/10.1073/pnas.0606150103

Wang, J., & Hamill, O. P. (2021). Piezo2—peripheral baroreceptor channel expressed in select neurons of the mouse brain: A putative mechanism for synchronizing neural networks by transducing intracranial pressure

pulses. *Journal of Integrative Neuroscience*, *20*(4), 825–837. https://doi.org/10.31083/j.jin2004085

Williamson, J. R., Tilton, R. G., Kilo, C., & Yu, S. (1980). Immunofluorescent imaging of capillaries and pericytes in human skeletal muscle and retina. *Microvascular Research*, *20*(2), 233–241. https://doi.org/10.1016/0026-2862(80)90010-2

Winship, I. R., Plaa, N., & Murphy, T. H. (2007). Rapid astrocyte calcium signals correlate with neuronal activity and onset of the hemodynamic response in vivo. *Journal of Neuroscience*, *27*(23), 6268–6272. https://doi.org/10.1523/jneurosci.4801-06.2007

Woo, S.-H., Lukacs, V., de Nooij, J. C., Zaytseva, D., Criddle, C. R., Francisco, A., Jessell, T. M., Wilkinson, K. A., & Patapoutian, A. (2015). Piezo2 is the principal mechanotransduction channel for proprioception. *Nature Neuroscience*, *18*(12), 1756–1762. https://doi.org/10.1038/nn.4162

Yang, G., & Iadecola, C. (1996). Glutamate microinjections in cerebellar cortex reproduce cerebrovascular effects of parallel fiber stimulation. *American Journal of Physiology-Regulatory, Integrative and Comparative Physiology*, *271*(6), R1568–R1575. https://doi.org/10.1152/ajpregu.1996.271.6.r1568

Yang, M.-F., Chien, C.-L., & Lu, K.-S. (1996). Morphological, immunohistochemical and quantitative studies of murine brain mast cells after mating. *Brain Research*, *846*(1), 30–39. https://doi.org/10.1016/s0006-8993(99)01935-6

Zeng, W.-Z., Marshall, K. L., Min, S., Daou, I., Chapleau, M. W., Abboud, F. M., Liberles, S. D., & Patapoutian, A. (2018). PIEZOs mediate neuronal sensing of blood pressure and the baroreceptor reflex. *Science*, *362*(6413), 464–467. https://doi.org/10.1126/science.aau6324

Zhang, F.-X., Ge, S.-N., Dong, Y.-L., Shi, J., Feng, Y.-P., Li, Y., Li, Y.-Q., & Li, J.-L. (2018). Vesicular glutamate transporter isoforms: The essential players in the somatosensory systems. *Progress in Neurobiology*, *171*, 72–89. https://doi.org/10.1016/j.pneurobio.2018.09.006

Zimmermann, K. W. (1923). Der feinere bau der blutcapillaren. *Zeitschrift für Anatomie und Entwicklungsgeschichte*, *68*(1), 29–109. https://doi.org/10.1007/bf02593544

Zonta, M., Angulo, M. C., Gobbo, S., Rosengarten, B., Hossmann, K.-A., Pozzan, T., & Carmignoto, G. (2002). Neuron-to-astrocyte signaling is central to the dynamic control of brain microcirculation. *Nature Neuroscience*, *6*(1), 43–50. https://doi.org/10.1038/nn980

**How to cite this article:** Larriva-Sahd, J., Martínez-Cabrera, G., Lozano-Flores, C., Concha, L., & Varela-Echavarría, A. (2023). The neurovascular unit of capillary blood vessels in the rat nervous system. A rapid-Golgi electron microscopy study. *Journal of Comparative Neurology*, 1–32. https://doi.org/10.1002/cne.25559